The Astrophysical Journal, 664:481–500, 2007 July 20

SPITZER: ACCRETION IN LOW-MASS STARS AND BROWN DWARFS IN THE λ ORIONIS CLUSTER[1]

David Barrado y Navascués
Laboratorio de Astrofísica Espacial y Física Fundamental, LAEFF-INTA, E-28080 Madrid, Spain; barrado@laeff.inta.es

John R. Stauffer
Spitzer Science Center, California Institute of Technology, Pasadena, CA 91125

María Morales-Calderón and Amelia Bayo
Laboratorio de Astrofísica Espacial y Física Fundamental, LAEFF-INTA, E-28080 Madrid, Spain

Giovanni Fazzio, Tom Megeath, and Lori Allen
Harvard Smithsonian Center for Astrophysics, Cambridge, MA 02138

and

Lee W. Hartmann and Nuria Calvet
Department of Astronomy, University of Michigan, Ann Arbor, MI 48109
Received 2006 October 3; accepted 2007 April 6

ABSTRACT

We present multiwavelength optical and IR photometry of 170 previously known low-mass stars and brown dwarfs of the 5 Myr Collinder 69 cluster (λ Orionis). The new photometry supports cluster membership for most of them, with less than 15% of the previous candidates identified as probable nonmembers. The near-IR photometry allows us to identify stars with IR excesses, and we find that the Class II population is very large, around 25% for stars (in the spectral range M0–M6.5) and 40% for brown dwarfs, down to 0.04 $M_{\odot}$, despite the fact that the Hα equivalent width is low for a significant fraction of them. In addition, there are a number of substellar objects, classified as Class III, that have optically thin disks. The Class II members are distributed in an inhomogeneous way, lying preferentially in a filament running toward the southeast. The IR excesses for the Collinder 69 members range from pure Class II (flat or nearly flat spectra longward of 1 μm), to transition disks with no near-IR excess but excesses beginning within the IRAC wavelength range, to two stars with excess only detected at 24 μm. Collinder 69 thus appears to be at an age where it provides a natural laboratory for the study of primordial disks and their dissipation.

Subject headings: open clusters and associations: individual (λ Orionis) — stars: low-mass, brown dwarfs — stars: pre–main-sequence

Online material: color figures

1. INTRODUCTION

The star formation process appears to operate successfully over a wide range of initial conditions. In regions like Taurus, groups of a few stars to a few tens of stars are the norm. The molecular gas in Taurus is arranged in a number of nearly parallel filaments, possibly aligned with the local magnetic field, and with the small stellar groups sited near endpoints of the filaments (Hartmann 2004). No high-mass stars have been formed in the Taurus groups, and the initial mass function (IMF) also appears to be relatively deficient in brown dwarfs (Briceño et al. 2003; Luhman 2004; but for an alternate view see also Guieu et al. 2006). The Taurus groups are not gravitationally bound and will disperse into the field on short timescales. At the other end of the mass spectrum, regions like the Trapezium cluster and its surrounding Orion Nebula cluster (ONC) have produced hundreds of stars. The ONC includes several O stars, with the earliest having spectral type O6 and an estimated mass of order 35 $M_{\odot}$. The very high stellar density in the ONC (10,000 stars pc^{-3} at its center; McCaughrean & Stauffer 1994) suggests that star formation in the ONC was gravity dominated rather than magnetic field dominated. It is uncertain whether the ONC is currently gravitationally bound or not, but it is presumably at least regions like the ONC that are the progenitors of long-lived open clusters like the Pleiades. UV photoionization and ablation from O star winds likely act to truncate the circumstellar disks of low-mass stars in the ONC, with potential consequences for giant planet formation.

An interesting intermediate scale of star formation is represented by the λ Ori association. The central cluster in the association, normally designated as Collinder 69 or the λ Orionis cluster, includes at least one O star, the eponymous λ Ori, with spectral type O8 III. However, a number of lines of evidence suggest that one of the Collinder 69 stars has already passed through its post–main-sequence evolution and become a supernova, hence indicating that it was more massive than λ Ori (see the complete IMF in Barrado y Navascués et al. 2005b). A census of the stars in Collinder 69 by Dolan & Mathieu (2001) indicates that the cluster is now strongly unbound. Dolan & Mathieu (2001) argue that this is due to rapid removal of molecular gas from the region that occurred about 1 Myr ago when the supernova exploded. They interpreted the color-magnitude diagram (CMD) of Collinder 69 as indicating a significant age spread with a maximum age of order 6 Myr; an alternative interpretation is that the cluster has negligible age spread (with age $\sim$6 Myr) and a significant number of

[1] Based on observations collected by the *Spitzer Space Telescope*, at the German-Spanish Astronomical Center of Calar Alto jointly operated by the Max-Planck-Institut für Astronomie Heidelberg and the Instituto de Astrofisica de Andalucía (CSIC), and at the WHT operated on the island of La Palma by the Isaac Newton Group in the Spanish Observatorio del Roque de los Muchachos of the Instituto de Astrofisica de Canarias.

binary stars. While Dolan & Mathieu (2001) identified a large population of low-mass stars in Collinder 69, only 4 of 72 for which they obtained spectra are classical T Tauri stars (based on their Hα emission equivalent widths). Much younger stars, including classical T Tauri stars, are present elsewhere in the λ Ori star formation rate (SFR), which Dolan & Mathieu (2001) attribute to star formation triggered by the supernova remnant shock wave impacting preexisting molecular cores in the region (the Barnard 30 and Barnard 35 dark clouds, in particular).

We have obtained *Spitzer Space Telescope* IRAC and MIPS imaging of a $\sim$1 deg^2 region centered on the star λ Ori in order to (1) search for circumstellar disks of members of the Collinder 69 cluster and (2) attempt to identify new, very low mass members of the cluster in order to determine better the cluster IMF (in a forthcoming paper). In § 2 we describe the new observations we have obtained; and in § 3 we use those data to reconsider cluster membership. In § 4 we use the new candidate member list and the IR photometry to determine the fraction of cluster members with circumstellar disks in both the stellar and substellar domain, and we sort the stars with disks according to their spectral slope from 1 to 24 μm.

2. THE DATA

2.1. *Optical and Near-Infrared Photometry*

The optical and the near-IR (NIR) data for the bright candidate members come from Barrado y Navascués et al. (2004, hereafter Paper I). The *RI* (Cousins system) data were collected with the Canada-France-Hawaii Telescope (CFHT) in 1999, whereas the *JHK*$_s$ data come from the Two Micron All Sky Survey (2MASS; Cutri et al. 2003[2]). For cluster members, the completeness limit is located at I(complete, cluster) $\sim$ 20.2 mag, whereas 2MASS provides NIR data down to a limiting magnitude of $J = 16.8$, $H = 16.5$, and $K_s = 15.7$ mag. In some cases, low-resolution spectroscopy in the optical, which provides spectral types and Hα equivalent widths, is also available. Twenty-five objects out of the 170 CFHT 1999 candidate members are in common with Dolan & Mathieu (1999, 2001). Those 25 stars also have Hα and lithium equivalent widths and radial velocities.

2.1.1. *New Deep Near-Infrared Photometry*

For the objects with large error in 2MASS *JHK*$_s$, or without this type of data due to their intrinsic faintness, we have obtained additional measurements with the WHT (La Palma Observatory, Spain) and INGRID ($4.1' \times 4.1'$ FOV) in 2002 November and 2003 February and with the Calar Alto 3.5 m telescope (Almeria, Spain) and Omega2000 in 2005 October ($15.36' \times 15.36'$ FOV). In all cases, for each position, we took five individual exposures of 60 s each, with small offsets of a few arcseconds, thus totaling 5 minutes. In the case of the campaigns with INGRID, we observed the area around the star λ Orionis creating a grid. Essentially, we have observed about $\frac{2}{3}$ of the CFHT 1999 optical survey region in J (in the area around the star and west of it), with some coverage in H and K. On the other hand, the Omega2000 observations, taken under a Director's Discretionary Time program, were focused on the faint candidate members. Except for one object (LOri 154), we collected observations in the J, H, and K_s filters. The conditions of the first observing run with INGRID were photometric, and we calibrated the data using standard stars from Hunt et al. (1998) observed throughout the nights of the run. The average seeing was 0.9″. We had cloud cover during the second run with INGRID, and the data were calibrated using the 2MASS

[2] Available at http://irsa.ipac.caltech.edu/applications/Gator/.

TABLE 1
Additional Near-Infrared Photometry for the Candidate Members of the λ Orionis Cluster (WHT/INGRID)

Name	I	J Error	H Error	K_s Error
LOri 006	12.752	11.67 ± 0.01	10.90 ± 0.01	10.94 ± 0.01
LOri 007	12.779	11.65 ± 0.01	...	...
LOri 008	12.789	11.53 ± 0.01	10.85 ± 0.01	10.62 ± 0.01
LOri 009	12.953	11.79 ± 0.01	...	...
LOri 011.....	13.006	11.59 ± 0.01	...	...
LOri 015	13.045	11.90 ± 0.01	...	...
LOri 016	13.181	12.00 ± 0.01	11.41 ± 0.01	11.27 ± 0.01
LOri 020	13.313	11.95 ± 0.01	...	...
LOri 021	13.376	12.26 ± 0.01	...	...
LOri 022	13.382	12.20 ± 0.01	11.44 ± 0.01	11.22 ± 0.01
LOri 024	13.451	12.35 ± 0.01	...	...
LOri 026	13.472	12.00 ± 0.01	...	...
LOri 027	13.498	12.51 ± 0.01	...	...
LOri 030	13.742	12.44 ± 0.01	11.81 ± 0.01	11.64 ± 0.01
LOri 031	13.750	12.34 ± 0.01	...	...
LOri 034	13.973	12.43 ± 0.01	...	...
LOri 035	13.974	12.56 ± 0.01	...	...
LOri 036	13.985	12.53 ± 0.01	...	...
LOri 037	13.988	13.43 ± 0.01	...	...
LOri 048	14.409	12.78 ± 0.01	12.17 ± 0.01	12.00 ± 0.01
LOri 049	14.501	13.13 ± 0.01	...	...
LOri 050	14.541	13.17 ± 0.01	...	...
LOri 053	14.716	13.17 ± 0.01	...	...
LOri 055	14.763	13.24 ± 0.01	...	...
LOri 056	14.870	13.33 ± 0.01	...	...
LOri 057	15.044	13.43 ± 0.01	...	...
LOri 060	15.144	13.60 ± 0.01	...	...
LOri 061	15.146	13.38 ± 0.01	12.74 ± 0.01	12.54 ± 0.01
LOri 062	15.163	13.60 ± 0.01	...	...
LOri 063	15.340	13.72 ± 0.01	13.02 ± 0.01	12.69 ± 0.01
LOri 065	15.366	13.66 ± 0.01	13.04 ± 0.01	12.85 ± 0.01
LOri 068	15.200	13.73 ± 0.01	...	...
LOri 069	15.203	13.28 ± 0.01	...	...
LOri 071	15.449	13.72 ± 0.01	...	...
LOri 073	15.277	13.68 ± 0.01	...	...
LOri 076	15.812	14.12 ± 0.01	13.51 ± 0.01	13.28 ± 0.01
LOri 077	15.891	14.11 ± 0.01	...	...
LOri 082	16.022	14.18 ± 0.01	13.64 ± 0.01	13.35 ± 0.01
LOri 083	16.025	14.22 ± 0.01	13.63 ± 0.01	13.32 ± 0.01
LOri 085	16.043	14.21 ± 0.01	13.58 ± 0.01	13.26 ± 0.01
LOri 087	16.091	14.44 ± 0.01	...	...
LOri 088	16.100	14.14 ± 0.01	...	...
LOri 089	16.146	14.43 ± 0.01	...	...
LOri 093	16.207	14.47 ± 0.01	...	...
LOri 094	16.282	14.37 ± 0.01	...	...
LOri 096	16.366	14.59 ± 0.01	13.98 ± 0.01	13.72 ± 0.01
LOri 099	16.416	14.62 ± 0.01	...	...
LOri 100	16.426	14.83 ± 0.01	...	...
LOri 102	16.505	14.57 ± 0.01	14.05 ± 0.01	13.78 ± 0.01
LOri 104	16.710	14.90 ± 0.01	...	...
LOri 105	16.745	14.84 ± 0.01	...	...
LOri 107	16.776	14.91 ± 0.01	14.35 ± 0.01	14.05 ± 0.01
LOri 115.....	17.077	15.35 ± 0.01	...	...
LOri 116.....	17.165	15.31 ± 0.01	...	...
LOri 120	17.339	15.36 ± 0.01	...	...
LOri 130	17.634	15.76 ± 0.01	...	...
LOri 131	17.783	15.29 ± 0.01	14.83 ± 0.01	14.41 ± 0.01
LOri 132	17.822	15.77 ± 0.01	...	...
LOri 134	17.902	15.72 ± 0.01	15.17 ± 0.01	14.82 ± 0.01
LOri 135	17.904	15.63 ± 0.01	15.14 ± 0.01	14.79 ± 0.01
LOri 136	17.924	15.53 ± 0.01	...	...

TABLE 2
Zero Points, Aperture Corrections, and Conversion Factors between the Magnitudes and the Fluxes in Jy

Channel	Ap. Correction ap = 4px (mag)	Ap. Correction ap = 2px (mag)	Zero Point[a] (mag)	Flux mag = 0 (Jy)
[3.6]	0.090	0.210	17.26	280.9[b]
[4.5]	0.102	0.228	16.78	179.7[b]
[5.8]	0.101	0.349	16.29	115.0[b]
[8.0]	0.121	0.499	15.62	64.1[b]
[24]	0.168[c]	0.168[c]	11.76	7.14[d]

[a] Zero points for aperture photometry performed with IRAF on the BCD data.
[b] Reach et al. (2005).
[c] The aperture used for MIPS [24] was always 5.31 pixels.
[d] Engelbracht et al. (2007).

catalog and the stars present in each individual image. The dispersion of this calibration is $\sigma = 0.05$ mag in each filter, with a seeing of about 1.0″. Finally, no standard stars were observed during the DDT observations at Calar Alto. The seeing in this case was 1.2″. The faint λ Orionis candidate members were calibrated using also 2MASS data. In this last case, the dispersion is somewhat higher, probably due to the worse seeing and the larger angular pixel scale of the detector, with $\sigma = 0.1$ mag. Note that this is dispersion, not the error in the calibration. These values correspond to the FWHM of the Gaussian distribution of the values zero point$(i) = \mathrm{mag}_{\mathrm{raw}}(i) - \mathrm{mag}_{\mathrm{2MASS}}(i)$, for any star i, which also includes the photometric errors in the 2MASS photometry and any contribution due to the cluster stars being photometrically variable. Since there are a large number of stars per field (up to 1000 in the Omega2000 images), the peak of this distribution can be easily identified and the zero points derived. A better estimate of the error in the calibration is based on the distance between mean, median, and mode values, which are smaller than half of the FWHM (in the case of the mean and the median, almost identical to the hundredth of magnitude). Therefore, the errors in the calibration can be estimated as 0.025 and 0.05 mag for the INGRID and the Omega2000 data sets, respectively.

All the data were processed and analyzed with IRAF[3] using aperture photometry. These measurements, for 166 candidate members, are listed in Table 1 (WHT/INGRID) and below in Table 3 (CAHA/Omega2000). Note that the errors listed in the table correspond to the values produced by the PHOT task with the digi.apphot package and do not include the errors in the calibrations.

2.2. *Spitzer Imaging*

Our *Spitzer* data were collected during 2004 March 15 (MIPS) and October 11 (IRAC) as part of a GTO program. The Infrared Array Camera (IRAC; Fazio et al. 2004) is a four-channel camera that takes images at 3.6, 4.5, 5.8, and 8.0 μm with a field of view that covers $\sim 5.2' \times 5.2'$. IRAC imaging was performed in mapping mode with individual exposures of 12 s "frametime" (corresponding to 10.4 s exposure times) and three dithers at each map step. In order to keep the total observation time for a given map under 3 hr, the λ Ori map was broken into two segments, each of size $28.75' \times 61.5'$, one offset west of the star λ Ori and the other offset to the east, with the combined image covering an area of $57' \times 61.5'$, leaving the star λ Orionis approximately at the center. Each of the IRAC images from the *Spitzer* Science Center pipeline was corrected for instrumental artifacts using an IDL routine developed by S. Carey and then combined into the mosaics at each of the four bandpasses using the MOPEX package (Makovoz & Khan 2005). Note that the IRAC images do not cover exactly the same FOV in all bands, providing a slice north of the star with data at 3.6 and 5.8 μm, and another slice south of it with photometry at 4.5 and 8.0 μm. The sizes of these strips are about $57' \times 6.7'$ in both cases. The Multiband Imaging Photometer for *Spitzer* (MIPS; Rieke et al. 2004) was used to map the cluster with a medium rate scan mode and 12 legs separated by 302″ in the cross scan direction. The total effective integration time per point on the sky at 24 μm for most points in the map was 40 s, and the mosaic covered an area of $60.5' \times 98.75'$ centered around the star λ Orionis. Since there were no visible artifacts in the pipeline mosaics for MIPS 24 μm, we used them as our starting point to extract the photometry. We obtained MIPS 70 and 160 μm imaging of the λ Ori region, but very few point sources were detected and we do not report those data in this paper.

The analysis of the data was done with IRAF. First, we detected objects in each image using the `starfind` command. Since the images in the [3.6] and [4.5] bands are deeper than those in the [5.8] and [8.0] bands, and since the fluxes of most objects are brighter at those wavelengths, the number of detections is much larger at the IRAC short wavelengths than at the longer ones. Only a relatively few objects have been detected at 24 μm with MIPS. As a summary, 164 objects were detected at 3.6 and 4.5 μm, 145 at 5.8 μm, 139 at 8.0 μm, and 13 at 24 μm.

We have performed aperture photometry to derive fluxes for Collinder 69 cluster members. For the IRAC mosaics we used an aperture of 4 pixel radius, and the sky was computed using a circular annulus 4 pixels wide, starting at a radius 4 pixels away from the center. It is necessary to apply an aperture correction to our 4 pixel aperture photometry in order to estimate the flux for a 10 pixel aperture because the latter is the aperture size used to determine the IRAC flux calibration. In some cases, due to the presence of nearby stars, hot pixels, or because of their faintness, a 2 pixel aperture and the appropriate aperture correction were used (see notes to Table 3). For the MIPS photometry at 24 μm, we used a 5.31 pixel (13″) aperture and a sky annulus from 8.16 pixels (20″) to 13.06 pixels (32″). An aperture correction was also applied. Table 2 provides the zero points, aperture corrections, and conversion factors between magnitudes and Jy, as provided by the *Spitzer* Science Center Web site.

2.2.1. *Data Cross-Correlation*

The coverage on the sky of our *Spitzer* IRAC data is an approximate square of about 1 deg^2, centered on the star λ Orionis. The optical data taken with the CFHT in 1999 cover an area of

[3] IRAF is distributed by National Optical Astronomy Observatory, which is operated by the Association of Universities for Research in Astronomy, Inc., under cooperative agreement with the National Science Foundation.

TABLE 3

PHOTOMETRY FOR CANDIDATE MEMBERS OF THE λ ORIONIS CLUSTER (COLLINDER 69)

Name	R Error	I Error	J Error	H Error	K_s Error	[3.6] Error	[4.5] Error	[5.8] Error	[8.0] Error	[24] Error	Mem.[a]
LOri 001	13.21 ± 0.00	12.52 ± 0.00	11.297 ± 0.022	10.595 ± 0.022	10.426 ± 0.021	10.228 ± 0.003	10.255 ± 0.004	10.214 ± 0.009	10.206 ± 0.010	...	Y
LOri 002	13.44 ± 0.00	12.64 ± 0.00	11.230 ± 0.024	10.329 ± 0.023	10.088 ± 0.019	9.935 ± 0.003	10.042 ± 0.003	9.930 ± 0.009	9.880 ± 0.008	...	Y
LOri 003	13.39 ± 0.00	12.65 ± 0.00	11.416 ± 0.023	10.725 ± 0.022	10.524 ± 0.023	10.262 ± 0.003	10.318 ± 0.004	10.239 ± 0.010	10.171 ± 0.010	...	Y
LOri 004	13.71 ± 0.00	12.65 ± 0.00	11.359 ± 0.022	10.780 ± 0.023	10.548 ± 0.021	10.287 ± 0.003	10.249 ± 0.004	10.185 ± 0.009	10.127 ± 0.009	...	Y
LOri 005	13.38 ± 0.00	12.67 ± 0.00	11.378 ± 0.022	10.549 ± 0.022	10.354 ± 0.023	10.204 ± 0.003	10.321 ± 0.004	10.218 ± 0.009	10.158 ± 0.009	...	Y
LOri 006	13.55 ± 0.00	12.75 ± 0.00	11.542 ± 0.026	10.859 ± 0.026	10.648 ± 0.021	10.454 ± 0.003	10.454 ± 0.004	10.399 ± 0.011	10.319 ± 0.010	...	Y
LOri 007	13.72 ± 0.00	12.78 ± 0.00	11.698 ± 0.027	11.101 ± 0.024	10.895 ± 0.030	10.668 ± 0.004	10.636 ± 0.004	10.615 ± 0.012	10.482 ± 0.013	...	Y
LOri 008	13.60 ± 0.00	12.79 ± 0.00	11.548 ± 0.029	10.859 ± 0.023	10.651 ± 0.024	10.498 ± 0.003	10.495 ± 0.004	10.440 ± 0.011	10.256 ± 0.012	...	Y
LOri 009	13.70 ± 0.00	12.95 ± 0.00	11.843 ± 0.024	11.109 ± 0.024	10.923 ± 0.023	10.834 ± 0.004	10.873 ± 0.005	10.788 ± 0.012	10.743 ± 0.014	...	Y
LOri 010	13.70 ± 0.00	12.96 ± 0.00	11.880 ± 0.026	11.219 ± 0.026	11.041 ± 0.023	10.916 ± 0.004	10.953 ± 0.005	10.733 ± 0.012	10.839 ± 0.016	...	Y
LOri 011	13.84 ± 0.00	13.01 ± 0.00	11.604 ± 0.026	10.784 ± 0.024	10.554 ± 0.024	10.378 ± 0.003	10.521 ± 0.004	10.444 ± 0.011	10.326 ± 0.011	...	Y
LOri 012	13.80 ± 0.00	13.03 ± 0.00	11.816 ± 0.026	10.971 ± 0.024	10.795 ± 0.023	10.619 ± 0.003	10.758 ± 0.005	10.627 ± 0.012	10.543 ± 0.012	...	Y
LOri 013	14.21 ± 0.00	13.03 ± 0.00	11.656 ± 0.022	10.918 ± 0.022	10.719 ± 0.023	10.511 ± 0.003	10.480 ± 0.004	10.467 ± 0.011	10.344 ± 0.012	...	Y
LOri 014	13.84 ± 0.00	13.03 ± 0.00	11.941 ± 0.024	11.278 ± 0.027	11.092 ± 0.023	10.902 ± 0.004	10.904 ± 0.005	10.839 ± 0.014	10.797 ± 0.014	...	Y
LOri 015	13.83 ± 0.00	13.05 ± 0.00	11.870 ± 0.024	11.127 ± 0.024	10.912 ± 0.019	10.808 ± 0.004	10.886 ± 0.005	10.824 ± 0.013	10.882 ± 0.015	...	Y
LOri 016	14.07 ± 0.00	13.18 ± 0.00	11.958 ± 0.024	11.284 ± 0.027	11.053 ± 0.024	10.833 ± 0.004	10.817 ± 0.006	10.378 ± 0.011	10.700 ± 0.014	...	Y
LOri 017	13.99 ± 0.00	13.19 ± 0.00	12.188 ± 0.024	11.482 ± 0.023	11.323 ± 0.021	11.165 ± 0.005	11.206 ± 0.006	11.173 ± 0.017	11.072 ± 0.019	...	Y
LOri 018	14.21 ± 0.00	13.26 ± 0.00	11.991 ± 0.024	11.284 ± 0.022	11.090 ± 0.023	10.804 ± 0.004	10.798 ± 0.005	10.722 ± 0.012	10.636 ± 0.014	...	Y
LOri 019	14.33 ± 0.00	13.31 ± 0.00	12.019 ± 0.026	11.316 ± 0.024	11.067 ± 0.021	10.880 ± 0.004	10.866 ± 0.005	10.767 ± 0.013	10.788 ± 0.018	...	Y
LOri 020	14.65 ± 0.00	13.31 ± 0.00	11.856 ± 0.028	11.214 ± 0.026	11.025 ± 0.027	10.676 ± 0.003	10.609 ± 0.004	10.573 ± 0.012	10.485 ± 0.012	...	Y
LOri 021	14.26 ± 0.00	13.38 ± 0.00	12.258 ± 0.027	11.560 ± 0.026	11.296 ± 0.021	11.129 ± 0.004	11.107 ± 0.005	11.081 ± 0.016	11.065 ± 0.019	...	Y
LOri 022	14.41 ± 0.00	13.38 ± 0.00	12.102 ± 0.023	11.411 ± 0.022	11.156 ± 0.019	11.010 ± 0.004	10.985 ± 0.005	10.895 ± 0.014	10.683 ± 0.014	...	Y
LOri 023	14.43 ± 0.00	13.44 ± 0.00	12.221 ± 0.027	11.471 ± 0.022	11.290 ± 0.024	11.090 ± 0.004	11.114 ± 0.005	11.071 ± 0.015	10.928 ± 0.018	...	Y
LOri 024	14.43 ± 0.00	13.45 ± 0.00	12.139 ± 0.030	11.446 ± 0.026	11.223 ± 0.028	11.018 ± 0.004	11.019 ± 0.005	10.972 ± 0.015	10.877 ± 0.016	...	Y
LOri 025	14.36 ± 0.00	13.45 ± 0.00	12.163 ± 0.044	11.409 ± 0.051	11.090 ± 0.033	10.668 ± 0.003	10.674 ± 0.004	10.613 ± 0.012	10.576 ± 0.012	...	Y
LOri 026	14.57 ± 0.00	13.47 ± 0.00	12.046 ± 0.028	11.324 ± 0.024	11.092 ± 0.025	10.882 ± 0.004	10.833 ± 0.005	10.811 ± 0.014	10.742 ± 0.013	...	Y
LOri 027	14.49 ± 0.00	13.50 ± 0.00	12.378 ± 0.026	11.718 ± 0.023	11.503 ± 0.021	11.305 ± 0.005	11.306 ± 0.006	11.237 ± 0.016	11.179 ± 0.025	...	Y
LOri 028	14.86 ± 0.00	13.65 ± 0.00	12.488 ± 0.024	11.872 ± 0.022	11.687 ± 0.021	11.439 ± 0.005	11.417 ± 0.006	11.348 ± 0.017	11.297 ± 0.021	...	Y
LOri 029	14.89 ± 0.00	13.69 ± 0.00	12.210 ± 0.026	11.460 ± 0.027	11.071 ± 0.019	10.259 ± 0.003	9.830 ± 0.003	9.321 ± 0.006	8.416 ± 0.003	5.684 ± 0.007	Y
LOri 030	14.95 ± 0.00	13.74 ± 0.00	12.427 ± 0.027	11.686 ± 0.026	11.428 ± 0.021	11.208 ± 0.007	11.157 ± 0.007	11.119 ± 0.019	10.997 ± 0.023	...	Y
LOri 031	14.90 ± 0.00	13.75 ± 0.00	12.412 ± 0.028	11.654 ± 0.023	11.442 ± 0.028	11.206 ± 0.004	11.188 ± 0.006	11.150 ± 0.015	11.079 ± 0.016	...	Y
LOri 032	15.04 ± 0.00	13.80 ± 0.00	12.410 ± 0.029	11.714 ± 0.023	11.493 ± 0.021	11.252 ± 0.004	11.215 ± 0.006	11.178 ± 0.016	11.080 ± 0.019	...	Y
LOri 033	14.82 ± 0.00	13.81 ± 0.00	12.455 ± 0.033	11.800 ± 0.042	11.502 ± 0.027	11.146 ± 0.004	11.149 ± 0.005	11.060 ± 0.015	11.020 ± 0.019	...	Y
LOri 034	15.10 ± 0.00	13.97 ± 0.00	12.442 ± 0.026	11.639 ± 0.026	11.184 ± 0.023	10.068 ± 0.003	9.734 ± 0.003	9.314 ± 0.007	8.325 ± 0.003	5.738 ± 0.007	Y
LOri 035	15.25 ± 0.00	13.97 ± 0.00	12.546 ± 0.024	11.842 ± 0.027	11.609 ± 0.019	11.371 ± 0.005	11.349 ± 0.006	11.283 ± 0.017	11.259 ± 0.021	...	Y
LOri 036	15.47 ± 0.00	13.98 ± 0.00	12.576 ± 0.024	11.936 ± 0.023	11.706 ± 0.021	11.395 ± 0.005	11.378 ± 0.006	11.287 ± 0.018	11.260 ± 0.019	...	Y
LOri 037	15.17 ± 0.00	13.99 ± 0.00	12.459 ± 0.024	11.727 ± 0.026	11.492 ± 0.021	11.302 ± 0.005	11.309 ± 0.006	11.198 ± 0.016	11.180 ± 0.018	...	Y
LOri 038	15.10 ± 0.00	14.01 ± 0.00	12.684 ± 0.030	11.954 ± 0.029	...	11.455 ± 0.005	11.320 ± 0.006	10.970 ± 0.014	9.857 ± 0.008	6.211 ± 0.010	Y
LOri 039	15.25 ± 0.00	14.02 ± 0.00	12.755 ± 0.030	12.004 ± 0.023	11.775 ± 0.023	11.523 ± 0.005	11.534 ± 0.007	11.434 ± 0.018	11.373 ± 0.025	...	Y
LOri 040	15.38 ± 0.00	14.06 ± 0.00	12.553 ± 0.024	11.877 ± 0.022	11.594 ± 0.024	11.364 ± 0.005	11.319 ± 0.006	11.231 ± 0.017	11.218 ± 0.025	...	Y
LOri 041	15.55 ± 0.00	14.10 ± 0.00	12.500 ± 0.024	11.856 ± 0.023	11.587 ± 0.027	11.255 ± 0.004	11.187 ± 0.006	11.131 ± 0.015	11.123 ± 0.021	...	Y
LOri 042	15.31 ± 0.00	14.14 ± 0.00	12.813 ± 0.027	12.099 ± 0.026	11.853 ± 0.023	11.604 ± 0.005	11.633 ± 0.007	11.546 ± 0.019	11.479 ± 0.025	...	Y
LOri 043	15.46 ± 0.00	14.16 ± 0.00	12.707 ± 0.024	12.021 ± 0.026	11.741 ± 0.024	11.512 ± 0.005	11.496 ± 0.007	11.408 ± 0.019	11.393 ± 0.024	8.479 ± 0.102	Y
LOri 044	15.39 ± 0.00	14.17 ± 0.00	12.924 ± 0.024	12.318 ± 0.024	12.065 ± 0.023	11.837 ± 0.006	11.804 ± 0.007	11.751 ± 0.023	11.674 ± 0.024	...	Y
LOri 045	15.56 ± 0.00	14.23 ± 0.00	12.768 ± 0.023	12.102 ± 0.026	11.844 ± 0.023	11.602 ± 0.005	11.596 ± 0.007	12.023 ± 0.039	11.474 ± 0.026	...	Y
LOri 046	15.64 ± 0.00	14.36 ± 0.00	13.033 ± 0.023	12.478 ± 0.026	12.252 ± 0.026	11.906 ± 0.006	11.852 ± 0.008	11.787 ± 0.024	11.763 ± 0.032	...	Y
LOri 047	15.91 ± 0.00	14.38 ± 0.00	12.732 ± 0.026	12.097 ± 0.031	11.827 ± 0.026	11.474 ± 0.005	11.400 ± 0.006	11.303 ± 0.017	11.342 ± 0.025	...	Y
LOri 048	15.78 ± 0.00	14.41 ± 0.00	12.887 ± 0.027	12.196 ± 0.029	11.932 ± 0.026	11.612 ± 0.006	11.521 ± 0.008	11.448 ± 0.020	10.920 ± 0.018	8.119 ± 0.087	Y

TABLE 3—*Continued*

Name	*R* Error	*I* Error	*J* Error	*H* Error	K_s Error	[3.6] Error	[4.5] Error	[5.8] Error	[8.0] Error	[24] Error	Mem.[a]
LOri 049	15.77 ± 0.00	14.50 ± 0.00	13.173 ± 0.027	12.592 ± 0.029	12.253 ± 0.023	12.004 ± 0.006	11.992 ± 0.009	12.043 ± 0.027	12.427 ± 0.057	...	Y
LOri 050	15.90 ± 0.00	14.54 ± 0.00	12.877 ± 0.027	12.236 ± 0.027	11.955 ± 0.031	11.471 ± 0.005	11.089 ± 0.005	10.529 ± 0.011	9.537 ± 0.007	7.268 ± 0.029	Y
LOri 051	15.91 ± 0.00	14.60 ± 0.00	13.266 ± 0.024	12.559 ± 0.022	12.285 ± 0.021	12.017 ± 0.006	11.995 ± 0.008	11.969 ± 0.024	11.919 ± 0.035	...	Y
LOri 052	15.93 ± 0.00	14.63 ± 0.00	13.117 ± 0.023	12.454 ± 0.024	12.192 ± 0.019	11.917 ± 0.006	11.863 ± 0.008	11.764 ± 0.022	11.791 ± 0.029	...	Y
LOri 053	16.08 ± 0.00	14.72 ± 0.00	13.173 ± 0.032	12.521 ± 0.023	12.278 ± 0.027	11.995 ± 0.006	11.954 ± 0.008	11.886 ± 0.022	11.862 ± 0.034	...	Y
LOri 054	16.19 ± 0.00	14.73 ± 0.00	13.189 ± 0.024	12.509 ± 0.022	12.271 ± 0.027	11.974 ± 0.006	11.948 ± 0.009	11.805 ± 0.025	11.862 ± 0.038	...	Y
LOri 055	16.12 ± 0.00	14.76 ± 0.00	13.184 ± 0.026	12.477 ± 0.026	12.253 ± 0.026	12.044 ± 0.006	12.038 ± 0.009	12.015 ± 0.029	11.902 ± 0.038	...	Y
LOri 056	16.43 ± 0.00	14.87 ± 0.00	13.211 ± 0.029	12.567 ± 0.026	12.267 ± 0.029	12.011 ± 0.004[b]	11.906 ± 0.005[b]	11.913 ± 0.019[b]	11.853 ± 0.032[b]	...	Y
LOri 057	16.63 ± 0.00	15.04 ± 0.00	13.412 ± 0.024	12.773 ± 0.023	12.487 ± 0.030	12.177 ± 0.007	12.078 ± 0.009	11.988 ± 0.030	11.992 ± 0.033	...	Y
LOri 058	16.57 ± 0.00	15.06 ± 0.00	13.521 ± 0.024	12.935 ± 0.022	12.643 ± 0.027	12.332 ± 0.007	12.269 ± 0.010	12.172 ± 0.032	12.637 ± 0.072	...	Y
LOri 059	16.57 ± 0.00	15.10 ± 0.00	13.574 ± 0.026	12.884 ± 0.026	12.682 ± 0.032	12.317 ± 0.007	12.270 ± 0.009	12.218 ± 0.030	12.679 ± 0.066	...	Y
LOri 060	16.56 ± 0.00	15.14 ± 0.00	13.598 ± 0.030	12.961 ± 0.030	12.663 ± 0.029	12.423 ± 0.008	12.418 ± 0.011	12.408 ± 0.041	12.377 ± 0.051	...	Y
LOri 061	16.58 ± 0.00	15.15 ± 0.00	13.533 ± 0.023	12.833 ± 0.026	12.525 ± 0.027	12.052 ± 0.006	11.851 ± 0.008	11.519 ± 0.019	10.730 ± 0.015	8.047 ± 0.046	Y
LOri 062	16.62 ± 0.00	15.16 ± 0.00	13.634 ± 0.029	13.005 ± 0.030	12.725 ± 0.027	12.370 ± 0.007	12.246 ± 0.009	12.153 ± 0.030	11.306 ± 0.021	7.834 ± 0.035	Y
LOri 063	16.80 ± 0.01	15.34 ± 0.00	13.756 ± 0.029	13.066 ± 0.029	12.663 ± 0.030	11.666 ± 0.006	11.368 ± 0.007	11.768 ± 0.028	10.397 ± 0.014	6.055 ± 0.010	Y
LOri 064	16.78 ± 0.01	15.34 ± 0.00	13.782 ± 0.026	13.098 ± 0.025	12.846 ± 0.029	12.486 ± 0.008	12.489 ± 0.011	12.378 ± 0.034	12.245 ± 0.053	...	Y
LOri 065	16.89 ± 0.01	15.37 ± 0.00	13.820 ± 0.024	13.123 ± 0.029	12.843 ± 0.027	12.526 ± 0.008	12.504 ± 0.011	12.494 ± 0.032	12.641 ± 0.063	8.424 ± 0.075	Y
LOri 066	17.12 ± 0.01	15.40 ± 0.00	13.506 ± 0.024	12.901 ± 0.026	12.654 ± 0.029	12.221 ± 0.007	12.170 ± 0.010	12.196 ± 0.039	12.578 ± 0.072	...	Y
LOri 067	17.05 ± 0.01	15.53 ± 0.00	14.000 ± 0.033	13.356 ± 0.027	13.102 ± 0.036	12.794 ± 0.010	12.727 ± 0.014	12.702 ± 0.046	12.786 ± 0.071	...	Y
LOri 068	16.76 ± 0.01	15.20 ± 0.00	13.521 ± 0.027	12.902 ± 0.026	12.628 ± 0.027	12.348 ± 0.005[b]	12.246 ± 0.006[b]	12.029 ± 0.016[b]	12.145 ± 0.036[b]	...	Y
LOri 069	16.89 ± 0.01	15.20 ± 0.00	13.384 ± 0.027	12.774 ± 0.027	12.425 ± 0.027	12.089 ± 0.006	12.015 ± 0.008	12.034 ± 0.026	11.903 ± 0.042	...	Y
LOri 070	17.18 ± 0.01	15.61 ± 0.00	14.042 ± 0.032	13.405 ± 0.029	13.067 ± 0.031	12.809 ± 0.009	12.779 ± 0.013	12.799 ± 0.041	12.559 ± 0.060	...	Y
LOri 071	17.13 ± 0.00	15.63 ± 0.00	13.749 ± 0.030	13.129 ± 0.024	12.839 ± 0.031	12.470 ± 0.008	12.382 ± 0.010	12.276 ± 0.031	12.250 ± 0.044	...	Y
LOri 072	17.00 ± 0.00	15.35 ± 0.00	13.554 ± 0.026	12.944 ± 0.032	12.631 ± 0.027	11.993 ± 0.006	11.860 ± 0.008	11.836 ± 0.026	11.718 ± 0.037	...	Y
LOri 073	16.84 ± 0.01	15.28 ± 0.00	13.644 ± 0.028	12.992 ± 0.023	12.715 ± 0.027	12.376 ± 0.007	12.274 ± 0.009	12.187 ± 0.029	12.162 ± 0.031	...	Y
LOri 074	17.03 ± 0.01	15.39 ± 0.00	13.663 ± 0.026	13.088 ± 0.025	12.720 ± 0.024	12.312 ± 0.007	12.310 ± 0.010	12.290 ± 0.030	12.259 ± 0.046	...	Y
LOri 075	16.95 ± 0.01	15.23 ± 0.00	13.396 ± 0.026	12.794 ± 0.026	12.526 ± 0.024	12.089 ± 0.006	11.990 ± 0.008	11.924 ± 0.026	11.936 ± 0.038	...	Y
LOri 076	17.39 ± 0.01	15.81 ± 0.00	14.216 ± 0.027	13.527 ± 0.027	13.201 ± 0.032	12.916 ± 0.010	12.843 ± 0.014	12.669 ± 0.048	12.754 ± 0.072	...	Y
LOri 077	17.45 ± 0.00	15.89 ± 0.00	14.031 ± 0.027	13.416 ± 0.027	13.109 ± 0.035	12.761 ± 0.009	12.717 ± 0.012	12.700 ± 0.046	12.650 ± 0.073	...	Y
LOri 078	17.35 ± 0.00	15.92 ± 0.00	14.227 ± 0.041	13.593 ± 0.053	13.286 ± 0.040	12.766 ± 0.009	12.844 ± 0.014	12.789 ± 0.046	12.554 ± 0.069	...	Y
LOri 079	17.51 ± 0.00	16.00 ± 0.00	14.221 ± 0.032	13.536 ± 0.032	13.338 ± 0.039	13.002 ± 0.006[b]	12.970 ± 0.008[b]	12.876 ± 0.078[b]	12.724 ± 0.048[b]	...	Y
LOri 080	17.51 ± 0.00	16.01 ± 0.00	13.804 ± 0.023	13.196 ± 0.022	12.891 ± 0.033	12.504 ± 0.008	12.424 ± 0.010	12.597 ± 0.041	12.190 ± 0.031	...	Y
LOri 081	17.61 ± 0.00	16.02 ± 0.00	14.669 ± 0.032	13.692 ± 0.032	13.209 ± 0.037	12.620 ± 0.008	12.360 ± 0.010	12.050 ± 0.030	11.632 ± 0.028	8.062 ± 0.056	Y
LOri 082	17.57 ± 0.00	16.02 ± 0.00	14.200 ± 0.033	13.570 ± 0.025	13.281 ± 0.033	13.008 ± 0.011	12.954 ± 0.015	13.586 ± 0.100	12.830 ± 0.100	...	Y
LOri 083	17.56 ± 0.00	16.02 ± 0.00	14.265 ± 0.030	13.638 ± 0.035	13.375 ± 0.040	13.012 ± 0.010	12.946 ± 0.013	12.947 ± 0.057	13.017 ± 0.074	...	Y
LOri 084	17.48 ± 0.00	16.03 ± 0.00	14.077 ± 0.024	13.448 ± 0.027	13.188 ± 0.034	12.888 ± 0.010	12.800 ± 0.013	12.863 ± 0.061	12.745 ± 0.067	...	Y
LOri 085	17.65 ± 0.01	16.04 ± 0.00	14.189 ± 0.026	13.622 ± 0.037	13.233 ± 0.027	12.584 ± 0.008	12.315 ± 0.010	12.090 ± 0.028	11.510 ± 0.029	8.089 ± 0.056	Y
LOri 086	17.59 ± 0.00	16.09 ± 0.00	14.482 ± 0.032	13.867 ± 0.032	13.503 ± 0.040	13.251 ± 0.011	13.205 ± 0.016	13.160 ± 0.057	13.277 ± 0.098	...	Y
LOri 087	17.54 ± 0.00	16.09 ± 0.00	14.186 ± 0.039	13.601 ± 0.030	13.279 ± 0.035	12.978 ± 0.010	12.894 ± 0.013	13.002 ± 0.064	12.669 ± 0.060	...	Y
LOri 088	17.78 ± 0.00	16.10 ± 0.00	14.140 ± 0.031	13.543 ± 0.037	13.228 ± 0.039	12.923 ± 0.009	12.853 ± 0.013	12.865 ± 0.040	12.676 ± 0.051	...	Y
LOri 089	17.79 ± 0.00	16.15 ± 0.00	14.380 ± 0.032	13.839 ± 0.035	13.512 ± 0.039	13.156 ± 0.011	13.123 ± 0.015	13.682 ± 0.086	12.877 ± 0.081	...	Y
LOri 090	17.77 ± 0.00	16.17 ± 0.00	14.515 ± 0.041	13.881 ± 0.023	13.651 ± 0.051	13.226 ± 0.011	13.116 ± 0.015	12.930 ± 0.047	13.126 ± 0.100	...	Y
LOri 091	18.01 ± 0.00	16.18 ± 0.00	14.184 ± 0.032	13.556 ± 0.032	13.289 ± 0.031	12.868 ± 0.009	12.803 ± 0.013	13.087 ± 0.062	12.462 ± 0.054	...	Y
LOri 092	17.84 ± 0.00	16.19 ± 0.00	14.441 ± 0.030	13.841 ± 0.038	13.537 ± 0.040	13.158 ± 0.011	13.053 ± 0.014	13.517 ± 0.087	12.992 ± 0.089	...	Y
LOri 093	17.82 ± 0.00	16.21 ± 0.00	14.462 ± 0.030	13.836 ± 0.039	13.604 ± 0.052	13.169 ± 0.011	13.104 ± 0.015	13.256 ± 0.073	12.982 ± 0.098	...	Y
LOri 094	18.03 ± 0.00	16.28 ± 0.00	14.404 ± 0.034	13.802 ± 0.030	13.425 ± 0.038	12.955 ± 0.009	12.994 ± 0.014	13.184 ± 0.058	12.894 ± 0.085	...	Y
LOri 095	17.96 ± 0.00	16.35 ± 0.00	14.564 ± 0.033	13.913 ± 0.029	13.613 ± 0.048	13.247 ± 0.012	13.278 ± 0.017	13.176 ± 0.067	13.340 ± 0.138	...	Y
LOri 096	18.02 ± 0.02	16.37 ± 0.00	14.627 ± 0.038	13.965 ± 0.037	13.638 ± 0.047	13.039 ± 0.010	12.732 ± 0.013	12.527 ± 0.045	12.029 ± 0.039	...	Y
LOri 098	18.12 ± 0.00	16.40 ± 0.00	14.647 ± 0.037	13.985 ± 0.045	13.682 ± 0.039	13.393 ± 0.012	13.301 ± 0.016	13.284 ± 0.075	13.182 ± 0.115	...	Y
LOri 099	18.14 ± 0.00	16.42 ± 0.00	14.709 ± 0.034	14.074 ± 0.035	13.676 ± 0.043	13.421 ± 0.013	13.335 ± 0.018	13.211 ± 0.069	13.352 ± 0.124	...	Y

TABLE 3—*Continued*

Name	*R* Error	*I* Error	*J* Error	*H* Error	K_s Error	[3.6] Error	[4.5] Error	[5.8] Error	[8.0] Error	[24] Error	Mem.[a]
LOri 100	18.08 ± 0.00	16.43 ± 0.00	14.768 ± 0.044	14.044 ± 0.042	13.821 ± 0.044	13.446 ± 0.012	13.325 ± 0.017	13.163 ± 0.066	13.318 ± 0.123	...	Y
LOri 101	18.14 ± 0.00	16.48 ± 0.00	15.019 ± 0.038	14.372 ± 0.044	14.110 ± 0.066	13.763 ± 0.015	13.627 ± 0.021	13.860 ± 0.105	13.475 ± 0.153	...	N
LOri 102	18.24 ± 0.00	16.50 ± 0.00	14.634 ± 0.047	14.083 ± 0.050	13.809 ± 0.057	13.296 ± 0.012	13.213 ± 0.015	13.275 ± 0.073	13.101 ± 0.108	...	Y
LOri 103	18.30 ± 0.00	16.55 ± 0.00	14.643 ± 0.029	14.126 ± 0.029	13.833 ± 0.055	13.425 ± 0.013	13.387 ± 0.018	13.140 ± 0.067	13.628 ± 0.151	...	Y
LOri 104	18.48 ± 0.03	16.71 ± 0.01	14.667 ± 0.030	14.136 ± 0.036	13.721 ± 0.042	13.143 ± 0.011	12.877 ± 0.014	12.694 ± 0.055	11.762 ± 0.035	...	Y
LOri 105	18.58 ± 0.00	16.75 ± 0.00	14.922 ± 0.040	14.340 ± 0.052	13.993 ± 0.053	13.621 ± 0.016	13.593 ± 0.021	13.601 ± 0.093	13.536 ± 0.159	...	Y
LOri 106	18.48 ± 0.00	16.76 ± 0.00	14.776 ± 0.043	14.161 ± 0.057	13.743 ± 0.045	13.295 ± 0.012	12.967 ± 0.014	12.558 ± 0.045	11.832 ± 0.034	8.849 ± 0.151	Y
LOri 107	18.85 ± 0.00	16.78 ± 0.00	14.656 ± 0.036	13.987 ± 0.035	13.621 ± 0.052	13.213 ± 0.017	13.152 ± 0.019	13.215 ± 0.082	13.046 ± 0.160	...	Y
LOri 108	18.64 ± 0.00	16.80 ± 0.00	14.840 ± 0.033	14.256 ± 0.048	13.918 ± 0.050	13.498 ± 0.013	13.464 ± 0.018	13.387 ± 0.073	13.303 ± 0.124	...	Y
LOri 109	18.67 ± 0.00	16.81 ± 0.00	14.96 ± 0.01	14.47 ± 0.01	14.18 ± 0.01	13.699 ± 0.015	13.654 ± 0.022	13.519 ± 0.077	13.708 ± 0.190	...	Y
LOri 110.....	18.54 ± 0.00	16.82 ± 0.00	15.043 ± 0.051	14.475 ± 0.056	14.144 ± 0.060	13.798 ± 0.016	13.796 ± 0.026	14.017 ± 0.130	13.454 ± 0.177	...	Y
LOri 111.....	18.88 ± 0.00	16.86 ± 0.00	14.801 ± 0.038	14.165 ± 0.043	13.786 ± 0.051	13.419 ± 0.012	13.330 ± 0.017	13.601 ± 0.082	13.664 ± 0.185	...	Y
LOri 112.....	18.72 ± 0.00	16.87 ± 0.00	14.991 ± 0.042	14.358 ± 0.048	14.148 ± 0.062	13.412 ± 0.013	13.335 ± 0.017	13.334 ± 0.079	13.299 ± 0.145	...	Y
LOri 113.....	18.71 ± 0.00	16.99 ± 0.00	15.18 ± 0.01	14.62 ± 0.01	14.30 ± 0.01	13.723 ± 0.017	13.579 ± 0.021	13.263 ± 0.070	12.448 ± 0.054	...	Y
LOri 114.....	18.99 ± 0.00	17.06 ± 0.00	15.092 ± 0.044	14.389 ± 0.053	14.006 ± 0.064	13.502 ± 0.015	13.414 ± 0.020	13.525 ± 0.096	13.051 ± 0.108	...	Y
LOri 115.....	18.80 ± 0.00	17.08 ± 0.00	15.449 ± 0.047	14.821 ± 0.068	14.594 ± 0.104	14.083 ± 0.017	14.012 ± 0.030	13.942 ± 0.119	13.346 ± 0.131	...	Y
LOri 116.....	19.05 ± 0.01	17.17 ± 0.00	15.343 ± 0.057	14.573 ± 0.055	14.411 ± 0.082	13.977 ± 0.017	13.847 ± 0.024	14.340 ± 0.190	13.614 ± 0.141	...	Y
LOri 117.....	19.24 ± 0.01	17.21 ± 0.00	15.10 ± 0.01	14.36 ± 0.01	14.17 ± 0.01	13.418 ± 0.018	13.102 ± 0.024	13.063 ± 0.105	...	...	Y
LOri 118.....	19.10 ± 0.01	17.23 ± 0.00	15.269 ± 0.044	14.686 ± 0.064	14.181 ± 0.057	13.430 ± 0.013	13.251 ± 0.016	12.844 ± 0.045	12.178 ± 0.043	...	Y
LOri 119.....	19.11 ± 0.00	17.30 ± 0.00	15.26 ± 0.01	14.74 ± 0.01	14.41 ± 0.01	13.568 ± 0.014	13.492 ± 0.019	13.408 ± 0.088	13.590 ± 0.170	...	Y
LOri 120	19.23 ± 0.00	17.34 ± 0.00	15.335 ± 0.050	14.770 ± 0.059	14.337 ± 0.087	13.878 ± 0.015	13.688 ± 0.020	13.458 ± 0.086	12.783 ± 0.070	...	Y
LOri 121	19.12 ± 0.00	17.37 ± 0.00	15.533 ± 0.060	15.093 ± 0.086	14.748 ± 0.099	14.336 ± 0.019	14.310 ± 0.031	14.053 ± 0.144	...	...	Y
LOri 122	19.31 ± 0.00	17.38 ± 0.00	15.428 ± 0.066	14.852 ± 0.060	14.462 ± 0.080	14.096 ± 0.018	13.973 ± 0.027	14.315 ± 0.190	13.659 ± 0.174	...	Y
LOri 124	19.30 ± 0.00	17.45 ± 0.00	15.661 ± 0.073	15.059 ± 0.082	14.778 ± 0.112	14.353 ± 0.012[b]	14.235 ± 0.018[b]	14.303 ± 0.086[b]	13.976 ± 0.126[b]	...	Y
LOri 125	19.29 ± 0.04	17.51 ± 0.01	15.661 ± 0.073	15.059 ± 0.082	14.778 ± 0.112	14.353 ± 0.012[b]	14.235 ± 0.018[b]	14.303 ± 0.086[b]	13.976 ± 0.126[b]	...	Y
LOri 126	19.52 ± 0.01	17.52 ± 0.00	15.62 ± 0.01	15.04 ± 0.01	14.67 ± 0.01	13.709 ± 0.014	13.577 ± 0.021	13.118 ± 0.063	12.352 ± 0.049	...	Y
LOri 127	19.87 ± 0.10	17.53 ± 0.01	13.016 ± 0.023	12.606 ± 0.027	12.468 ± 0.024	12.401 ± 0.007	12.348 ± 0.010	12.301 ± 0.033	12.352 ± 0.037	...	N
LOri 128	19.53 ± 0.01	17.58 ± 0.00	15.624 ± 0.077	15.099 ± 0.087	14.769 ± 0.109	14.150 ± 0.021	14.115 ± 0.031	14.327 ± 0.254	13.956 ± 0.209	...	Y
LOri 129	19.51 ± 0.01	17.59 ± 0.00	15.383 ± 0.056	14.816 ± 0.072	14.526 ± 0.102	13.625 ± 0.014	13.317 ± 0.016	13.194 ± 0.058	12.598 ± 0.057	...	Y
LOri 130	19.44 ± 0.01	17.63 ± 0.00	15.731 ± 0.059	15.265 ± 0.092	14.735 ± 0.110	14.408 ± 0.013[b]	14.382 ± 0.020[b]	14.041 ± 0.077[b]	14.348 ± 0.256[b]	...	Y
LOri 131	19.79 ± 0.01	17.78 ± 0.00	15.429 ± 0.054	14.900 ± 0.063	14.380 ± 0.090	13.991 ± 0.017	13.909 ± 0.025	13.865 ± 0.119	13.344 ± 0.106	...	Y
LOri 132	19.99 ± 0.01	17.82 ± 0.00	15.583 ± 0.067	14.962 ± 0.078	14.913 ± 0.145	14.173 ± 0.019	14.087 ± 0.025	14.076 ± 0.140	13.630 ± 0.129	...	Y
LOri 133	19.68 ± 0.01	17.83 ± 0.00	16.290 ± 0.101	15.900 ± 0.167	15.378 ± 0.203	15.066 ± 0.032	14.941 ± 0.041	15.077 ± 0.312	...	...	N
LOri 134	19.91 ± 0.01	17.90 ± 0.00	15.543 ± 0.057	14.937 ± 0.074	14.666 ± 0.107	14.321 ± 0.020	14.071 ± 0.027	13.880 ± 0.113	13.884 ± 0.154	...	Y
LOri 135	19.91 ± 0.01	17.90 ± 0.00	15.671 ± 0.072	15.082 ± 0.087	14.908 ± 0.138	14.334 ± 0.014[b]	14.166 ± 0.018[b]	14.171 ± 0.113[b]	13.871 ± 0.108[b]	...	Y
LOri 136	20.06 ± 0.12	17.92 ± 0.01	15.560 ± 0.085	14.828 ± 0.090	14.576 ± 0.108	14.139 ± 0.016[b]	14.224 ± 0.023[b]	13.948 ± 0.083[b]	13.607 ± 0.107[b]	...	Y
LOri 137	19.89 ± 0.08	17.96 ± 0.09	...	...	...	16.454 ± 0.073	16.789 ± 0.270	...	...	...	N
LOri 138	20.01 ± 0.01	17.96 ± 0.00	15.821 ± 0.078	15.204 ± 0.083	14.971 ± 0.133	14.527 ± 0.022	14.469 ± 0.035	14.150 ± 0.123	...	...	Y
LOri 139	20.04 ± 0.01	18.16 ± 0.00	16.16 ± 0.01	15.53 ± 0.01	15.06 ± 0.01	14.054 ± 0.017	13.658 ± 0.019	13.151 ± 0.056	12.663 ± 0.062	...	Y
LOri 140	20.34 ± 0.01	18.21 ± 0.00	15.981 ± 0.078	15.224 ± 0.089	14.750 ± 0.113	14.030 ± 0.017	13.704 ± 0.023	13.299 ± 0.066	12.786 ± 0.078	...	Y
LOri 141	20.44 ± 0.01	18.25 ± 0.00	16.61 ± 0.01	15.89 ± 0.01	15.68 ± 0.02	15.100 ± 0.034	15.668 ± 0.089	...	...	...	N
LOri 142	20.34 ± 0.01	18.27 ± 0.00	16.25 ± 0.01	15.58 ± 0.01	15.26 ± 0.01	14.705 ± 0.028	14.674 ± 0.041	...	...	...	Y
LOri 143	20.32 ± 0.01	18.30 ± 0.00	16.11 ± 0.01	15.61 ± 0.02	15.23 ± 0.01	14.835 ± 0.015	14.896 ± 0.023	14.765 ± 0.089	14.553 ± 0.126	...	Y
LOri 144	20.24 ± 0.11	18.30 ± 0.11	17.69 ± 0.02	16.90 ± 0.02	16.55 ± 0.03	16.476 ± 0.094	16.424 ± 0.184	...	...	...	N?
LOri 146	20.88 ± 0.26	18.60 ± 0.02	16.230 ± 0.107	15.470 ± 0.110	14.936 ± 0.128	14.404 ± 0.022[b]	14.199 ± 0.035[b]	13.836 ± 0.103[b]	13.614 ± 0.175[b]	...	Y
LOri 147	20.54 ± 0.01	18.60 ± 0.00	16.58 ± 0.02	15.93 ± 0.02	15.62 ± 0.02	15.348 ± 0.023[b]	15.675 ± 0.048[b]	15.128 ± 0.224[b]	...	...	Y?
LOri 148	20.77 ± 0.02	18.62 ± 0.00	16.39 ± 0.01	16.12 ± 0.01	15.98 ± 0.02	14.869 ± 0.030	14.989 ± 0.051	14.530 ± 0.210	...	...	Y?
LOri 149	21.07 ± 0.02	18.95 ± 0.00	99.99 ± 0.00	88.88 ± 0.00	16.97 ± 0.02	17.135 ± 0.132[b]	16.829 ± 0.099[b]	...	...	...	N

TABLE 3—*Continued*

Name	*R* Error	*I* Error	*J* Error	*H* Error	K_s Error	[3.6] Error	[4.5] Error	[5.8] Error	[8.0] Error	[24] Error	Mem.[a]
LOri 150	21.29 ± 0.03	19.00 ± 0.00	16.656 ± 0.152	16.134 ± 0.197	15.560 ± 0.214	15.015 ± 0.032	15.133 ± 0.070	14.942 ± 0.390	...	...	Y
LOri 151	20.98 ± 0.02	19.00 ± 0.00	17.40 ± 0.02	16.76 ± 0.02	16.52 ± 0.04	15.801 ± 0.056	15.716 ± 0.103	...	...	...	N
LOri 152	21.43 ± 0.04	19.05 ± 0.00	16.773 ± 0.173	16.657 ± 0.295	15.870 ± 0.285	16.313 ± 0.086	16.316 ± 0.158	...	...	...	N?
LOri 153	21.30 ± 0.03	19.17 ± 0.00	17.09 ± 0.01	16.37 ± 0.01	16.09 ± 0.03	15.223 ± 0.036	15.139 ± 0.072	...	...	...	Y
LOri 154	21.79 ± 0.05	19.31 ± 0.00	16.804 ± 0.169	16.143 ± 0.192	15.513 ± 0.219	15.071 ± 0.035	15.953 ± 0.141	...	...	...	Y
LOri 155	21.87 ± 0.06	19.36 ± 0.00	16.97 ± 0.01	16.30 ± 0.01	15.84 ± 0.02	15.085 ± 0.019[b]	15.412 ± 0.045[b]	14.878 ± 0.163[b]	14.517 ± 0.183[b]	...	Y
LOri 156	22.05 ± 0.06	19.59 ± 0.01	17.06 ± 0.02	16.34 ± 0.02	15.89 ± 0.02	14.942 ± 0.029	14.688 ± 0.038	14.127 ± 0.148	13.870 ± 0.146	...	Y
LOri 157	22.09 ± 0.06	19.63 ± 0.01	18.08 ± 0.03	17.42 ± 0.03	17.00 ± 0.04	16.907 ± 0.103	16.719 ± 0.161	...	...	...	N
LOri 158	22.07 ± 0.05	19.67 ± 0.01	18.59 ± 0.03	17.86 ± 0.05	17.61 ± 0.08	17.627 ± 0.123[b]	17.565 ± 0.245[b]	...	...	...	N?
LOri 159	22.25 ± 0.06	20.01 ± 0.01	18.21 ± 0.02	17.62 ± 0.05	17.47 ± 0.09	16.422 ± 0.089	16.627 ± 0.207	...	...	...	N?
LOri 160	22.82 ± 0.13	20.29 ± 0.02	18.11 ± 0.03	17.14 ± 0.02	16.38 ± 0.03	15.669 ± 0.052	15.384 ± 0.079	...	...	...	Y
LOri 161	23.09 ± 0.19	20.34 ± 0.01	17.71 ± 0.02	16.90 ± 0.02	16.51 ± 0.03	16.361 ± 0.122	16.451 ± 0.249	...	...	...	Y
LOri 162	23.22 ± 0.51	20.42 ± 0.02	17.64 ± 0.03	16.90 ± 0.09	16.52 ± 0.04	15.675 ± 0.062	15.733 ± 0.112	...	...	...	Y
LOri 163	22.96 ± 0.24	20.42 ± 0.02	17.86 ± 0.04	17.02 ± 0.08	16.76 ± 0.05	15.666 ± 0.062	15.904 ± 0.119	...	...	...	Y
LOri 164	23.11 ± 0.17	20.44 ± 0.01	18.75 ± 0.04	18.17 ± 0.05	18.31 ± 0.13	...	...	...	...	...	N
LOri 165	23.12 ± 0.22	20.73 ± 0.02	18.77 ± 0.08	18.11 ± 0.16	17.90 ± 0.09	16.377 ± 0.112	16.130 ± 0.189	...	...	...	N?
LOri 166	23.33 ± 0.18	20.75 ± 0.02	18.26 ± 0.03	88.88 ± 0.00	17.38 ± 0.04	16.655 ± 0.055[b]	17.232 ± 0.237[b]	...	...	...	Y?
LOri 167	23.86 ± 0.64	20.90 ± 0.02	18.01 ± 0.03	17.17 ± 0.07	16.83 ± 0.09	15.935 ± 0.063	16.060 ± 0.129	...	...	...	Y
LOri 168	24.15 ± 0.62	21.54 ± 0.04	19.39 ± 0.09	18.58 ± 0.08	18.70 ± 0.25	...	...	...	...	...	N?
LOri 169	24.83 ± 1.10	21.88 ± 0.05	20.10 ± 0.10	19.47 ± 0.15	018.93 ± 0.42	...	...	...	...	...	Y?
LOri 170	25.41 ± 2.61	22.06 ± 0.07	20.35 ± 0.20	19.20 ± 0.20	019.39 ± 0.46	...	...	...	...	...	N?

NOTES.—LOri 097 and LOri 145 are artifacts. LOri 123 is a nonmember and has uncertainties in its photometry.

[a] Final membership.

[b] The 2 pixel aperture radius used for the photometry due to the presence of nearby objects or hot pixels.

$42' \times 28'$, again leaving the star in the center of this rectangle. Therefore, the optical survey is completely included in the *Spitzer* mapping, and we have been able to look for the counterpart of the cluster candidates presented in Paper I. The analysis of the area covered by *Spitzer* but without optical imaging in the CFHT 1999 survey will be discussed in a forthcoming paper. We have not been able to obtain reliable *Spitzer* photometry for some candidate members from Paper I, especially at the faint end of the cluster sequence. The faintest detected object, LOri 167, depending on the isochrone and the model, would have a mass of $\sim$0.017 $M_{\odot}$, if it is a member (Barrado y Navascués et al. 2005a).

The results are listed in Table 3, where nonmembers and members are included, respectively (see next section for the discussion about the membership). In both cases, we include data corresponding to the bands R and I (from CFHT), J, H, and K_s (from 2MASS and CAHA), [3.6], [4.5], [5.8], and [8.0] (from IRAC), and [24] (from MIPS). Additional NIR photometry from WHT can be found in Table 1.

3. COLOR-COLOR AND COLOR-MAGNITUDE DIAGRAMS AND NEW MEMBERSHIP ASSIGNMENT

Before discussing membership of the Paper I stars based on all of the new optical and IR data, we have made an initial selection based on the IRAC colors. Figure 1 (see further discussion in the next section) displays a color-color diagram with the four IRAC bands. We have found that 31 objects fall in the area defined by Allen et al. (2004) and Megeath et al. (2004) as Class II objects (i.e., T Tauri stars). Another two candidate members are located in the region corresponding to Class I/II objects. We consider all these 33 objects as bona fide members of the Collinder 69 cluster. Harvey et al. (2006) have discussed the confusion by extragalactic and other sources when analyzing *Spitzer* data (in their case, they used Serpens, a cloud having a large extinction). We believe that this contribution is negligible for our λ Ori data, since those Class II objects detected at 24 μm are in the T Tauri area defined by Sicilia-Aguilar et al. (2005) as displayed in their Figure 5. There can be a higher level of contamination among the objects classified as Class III. All of the objects in Figure 1 had previously been identified as cluster candidate members based on optical CMDs: it is unlikely that a significant number of active galactic nuclei would have passed both our optical and our IR criteria (and also have been unresolved in our optical CFHT images). Moreover, prior to our *Spitzer* data, only 25% of candidate members that had optical and NIR data and optical low-resolution spectroscopy turned out to be nonmembers (Paper I). After adding the *Spitzer* photometry, we are quite confident in the membership of the selection.

Figures 2 and 3 display several CMDs using the data listed in Tables 1 and 3. In the case of the panels of the first figure, we present optical and IR, including *Spitzer* IRAC data, whereas in the second set of figures only IR data are plotted. For the sake of simplicity, we have also removed the nonmembers from Figure 3.

Based on these diagrams and on the spectroscopic information included in Paper I, we have reclassified the candidate members as belonging or not to the cluster. In CMDs, Collinder 69 members lie in a fairly well defined locus, with a lower bound that coincides approximately with the 20 Myr isochrone in this particular set of theoretical models (Baraffe et al. 1998). Stars that fall well below (or blueward) of that locus are likely nonmembers; stars that fall above or redward of that locus are retained because they could have IR excesses or above average reddening. We combine the "votes" from several CMDs to yield a qualitative membership determination, essentially yes, no, or maybe. In total, out of 170 candidates, 19 are probable nonmembers, 4 have dubious

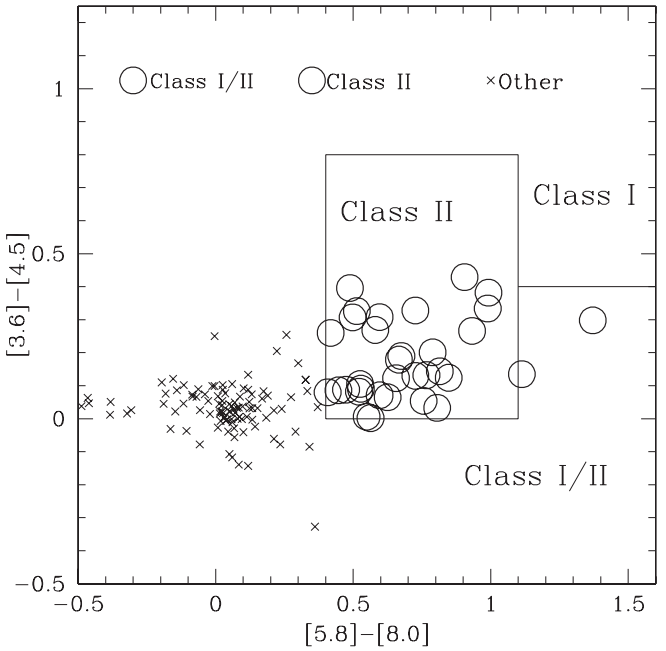

FIG. 1.—*Spitzer* IRAC CCD. Class I/II (*large open circles*), Class II (*large open circles*), and Class III (or nonmembers; *crosses*) have been classified using this diagram (after Allen et al. 2004; Hartmann et al. 2005). [*See the electronic edition of the Journal for a color version of this figure.*]

membership, and the rest (147 objects) seem to be bona fide members of the cluster. Therefore, the ratio of nonmembers to initial candidate members is 13.5%. In any case, only additional spectroscopy (particularly medium and high resolution) can be used to establish the real status. Proper motion might be helpful, but as shown by Bouy et al. (2007), some bona fide member can appear to have discrepant proper motions when compared with the average values of the association. Table 4 shows the results for each candidate in the different tests used to determine its membership, the membership as in Paper I, and the final membership based on the new photometry. The second and last columns show the spectroscopic information. Note that the degree of confidence in the new membership classification varies depending on the available information, and in any event it is always a matter of probability.

As Table 3 shows, the *Spitzer* IRAC data do not match completely the limiting magnitudes of either our optical survey with CFHT or the 2MASS JHK_s data. In the case of the band [3.6], essentially all the λ Orionis candidate members should have been detected (except perhaps the faintest ones, at about $I = 22$ mag). Some objects in the faint end have 3.6 μm data but lack 2MASS NIR, although in most cases we have supplied it with our own deep NIR survey. In the case of the *Spitzer* data at 4.5 μm, some additional candidate members fainter than $I = 20.9$ mag were not found, due to the limiting magnitude of about $[4.5]_{\rm lim} = 16.3$ mag. The data at 8.0 μm only reach $[8.0]_{\rm lim} = 14.0$ mag, which means that only cluster members with about $I = 18.6$ mag (or $K_s = 14.9$) can be detected at that wavelength. This is important when discussing both the membership status based on CMDs and the presence of infrared excesses by examining color-color diagrams (CCDs). Note, however, that objects with IR excesses have fainter optical/NIR counterparts than predicted in the table.

Figure 4 presents another CMD with the optical magnitudes from the CFHT survey (R and I), where we display the 170 candidate members using different symbols to distinguish their actual membership status. Small filled circles correspond to nonmembers based on the previous discussion, whereas plus signs, crosses, and

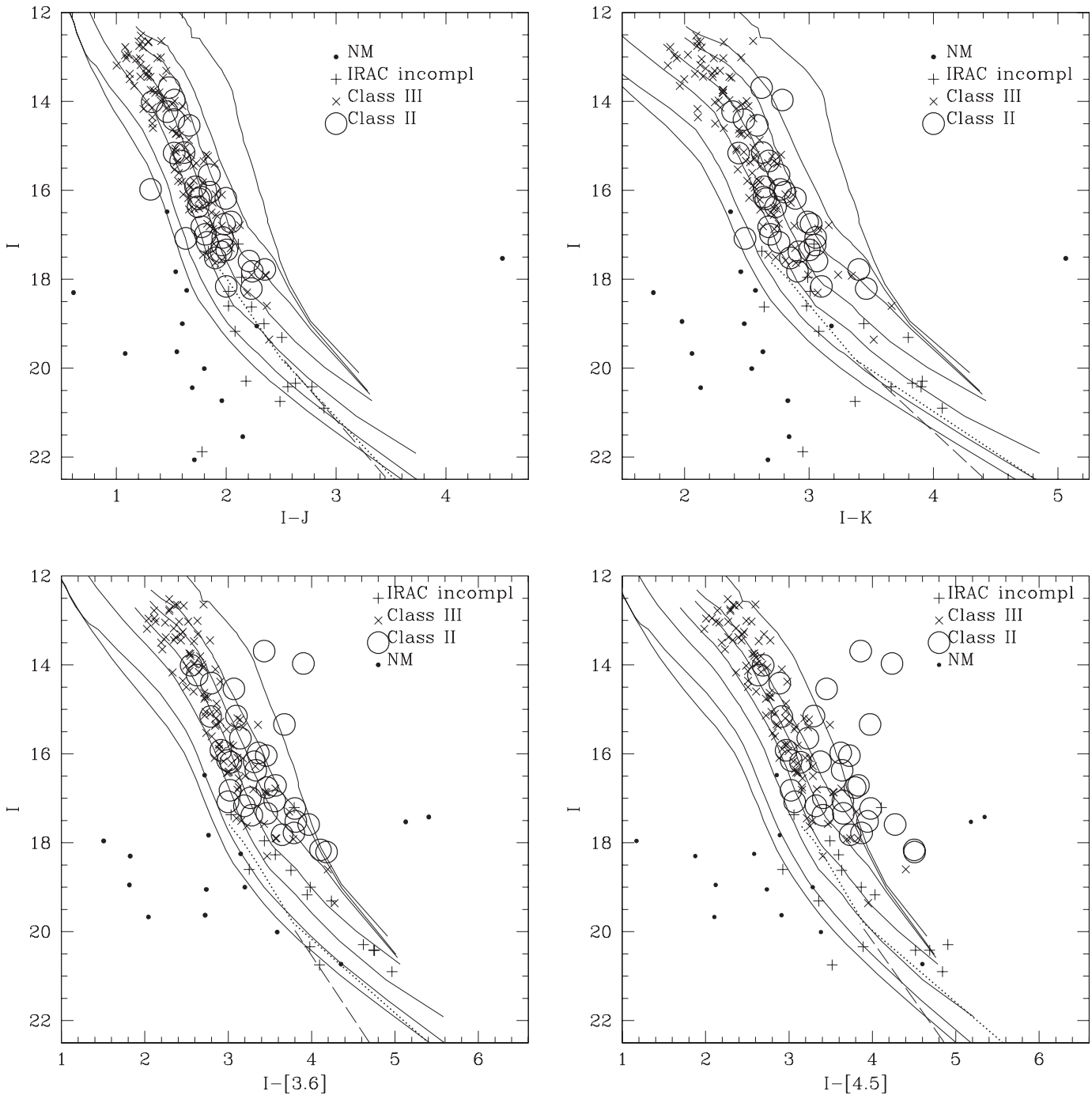

FIG. 2.—Optical/IR CMD. Nonmembers appear as small filled circles. Class II sources (classical T Tauri stars and substellar analogs) have been included as large open circles, whereas Class III (weak-line T Tauri) objects appear as crosses, and other λ Orionis members lacking the complete set of IRAC photometry are displayed with plus signs. The figure includes 1, 3, 5, 10, 20, 50, and 100 Myr isochrones from Baraffe et al. (1998) as solid lines, as well as 5 Myr isochrones corresponding to DUSTY and COND models (Chabrier et al. 2000; Baraffe et al. 2002) as dotted and dashed lines, respectively. [*See the electronic edition of the Journal for a color version of this figure.*]

large open circles denote probable members. In the first case (in most cases due to their faintness) they do not have a complete set of IRAC magnitudes, although they can have a measurement at 3.6 and 4.5 μm, or even at 5.8 μm. In the case of the objects represented by crosses, they have been classified as Class III objects (weak-line T Tauri stars and substellar analogs if they indeed belong to the cluster) based on an IRAC CCD (see next section and Fig. 1). Finally, large open circles correspond to Class II sources. The pollution rate seems to be negligible in the magnitude range $I = 12$–16 (1.2–0.17 $M_{\odot}$ approximately, equivalent to M0 and M5, respectively), where our initial selection based on the optical and the NIR (2MASS data) has worked nicely. However, for fainter candidates, the number of spurious members is very large and the pollution rate amounts to about 15% for objects with $16 < I < 19$ and about 45% for $I \geq 19$ (approximately the magnitude beyond the reach of the 2MASS).

At a distance of 400 pc and for an age of 5 Myr, and according to the models by Baraffe et al. (1998), the substellar borderline is located at about $I = 17.5$ mag. Table 5 lists other values for different ages, as well as other bands (J, K_s, and L') discussed in this paper. Among our 170 CFHT candidate members, there are 25 objects fainter than that magnitude and that pass all of our membership criteria that are probable brown dwarfs. Out of these 25 objects, 12 have low-resolution spectroscopy and seem to be bona fide

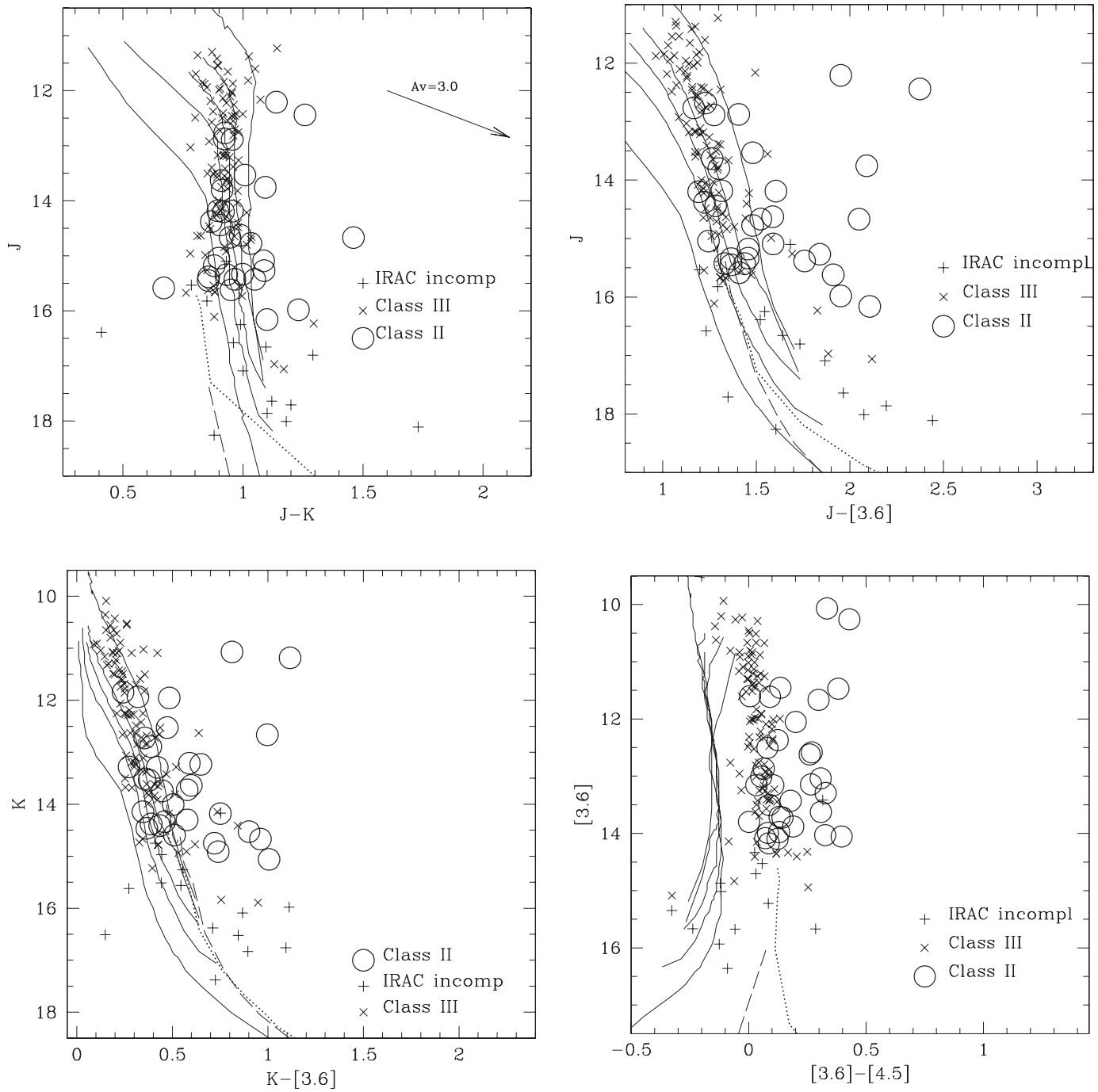

FIG. 3.—NIR and *Spitzer* CMD. Class II sources (classical T Tauri stars and substellar analogs) have been included as large open circles, whereas Class III (weak-line T Tauri) objects appear as crosses, and other λ Orionis members lacking the complete set of IRAC photometry are displayed with plus signs. The figure includes 1, 5, 10, 20, and 100 Myr isochrones from Baraffe et al. (1998) as solid lines, as well as 5 Myr isochrones corresponding to DUSTY and COND models (Chabrier et al. 2000; Baraffe et al. 2002) as dotted and dashed lines, respectively. Note that in the last panel we have the L and M data for the NextGen models, since *Spitzer* photometry has not been computed for this set of models. [*See the electronic edition of the Journal for a color version of this figure.*]

members and, therefore, brown dwarfs. The other 13 objects are waiting for spectral confirmation of their status. Assuming an age of 3 or 8 Myr would increase or decrease the number of brown dwarfs by seven in each case. In the first case (3 Myr), five out of the seven possible brown dwarfs have spectroscopic membership, whereas in the second case only three were observed in Paper I. As a summary, we have found between 18 and 32 good brown dwarf candidates (depending on the final age) in the λ Orionis cluster, and between 17 and 9 have their nature confirmed via low-resolution spectroscopy. Note that even this technique does not preclude the possibility that a few among them would actually be nonmembers.

Finally, the planetary mass domain starts at about $I_C = 21.5$, using a 5 Myr isochrone (DUSTY models from Baraffe et al. 2002). In that region, there is only one promising planetary mass candidate, LOri 167 (Barrado y Navascués et al. 2007).

4. DISCUSSION

4.1. *The Color-Color Diagrams, the Diagnostic of IR Excess, and the Disk Ratio*

The *Spitzer* IRAC colors are a powerful tool to reveal the dust and, therefore, the population of Class I and II sources in a stellar

TABLE 4

MEMBERSHIP AND OTHER PROPERTIES OF CANDIDATE MEMBERS OF THE λ ORIONIS CLUSTER (COLLINDER 69)

Name	Spectral Type	Phot. Mem.[a]	Paper I Mem.	Final Mem.	IRAC Classification[b]	SED Slope[c]	Disk Type	Comment[d]
LOri 001	...	Y Y Y Y Y Y Y	Mem	Y	III	−2.8	Diskless	Ha− WHa(DM)=2.51 DM 01
LOri 002	...	Y Y Y Y Y Y Y	NM−	Y	III	−2.74	Diskless	
LOri 003	...	Y Y Y Y Y Y Y	Mem	Y	III	−2.71	Diskless	Ha− WHa(DM)=3.35 DM#46
LOri 004	...	Y Y Y Y Y Y Y	Mem	Y	III	−2.65	Diskless	
LOri 005	...	Y Y Y Y Y Y Y	NM−	Y	III	−2.75	Diskless	
LOri 006	...	Y Y Y Y Y Y Y	Mem	Y	III	−2.68	Diskless	
LOri 007	...	Y Y Y Y Y Y Y	Mem	Y	III	−2.63	Diskless	
LOri 008	...	Y Y Y Y Y Y Y	Mem	Y	III	−2.56	Diskless	Ha− WHa(DM)=1.65 DM#51
LOri 009	...	Y Y Y Y Y Y Y	Mem	Y	III	−2.71	Diskless	
LOri 010	...	Y Y Y Y Y Y Y	Mem	Y	III	−2.69	Diskless	
LOri 011	...	Y Y Y Y Y Y Y	NM−	Y	III	−2.70	Diskless	
LOri 012	...	Y Y Y Y Y Y Y	NM−	Y	III	−2.70	Diskless	
LOri 013	...	Y Y Y Y Y Y Y	Mem	Y	III	−2.66	Diskless	Ha− WHa(DM)=4.41 DM#04
LOri 014	...	Y Y Y Y Y Y Y	Mem	Y	III	−2.71	Diskless	Ha− WHa(DM)=1.45 DM#58
LOri 015	...	Y Y Y Y Y Y Y	Mem	Y	III	−2.89	Diskless	
LOri 016	...	Y Y Y Y Y Y Y	Mem	Y	III	−2.58	Diskless	
LOri 017	...	Y Y Y Y Y Y Y	Mem	Y	III	−2.72	Diskless	Ha− WHa(DM)=0.80 DM#60
LOri 018	...	Y Y Y Y Y Y Y	Mem	Y	III	−2.63	Diskless	Ha− WHa(DM)=2.02 DM#56
LOri 019	...	Y Y Y Y Y Y Y	Mem	Y	III	−2.71	Diskless	
LOri 020	...	Y Y Y Y Y Y Y	Mem	Y	III	−2.63	Diskless	
LOri 021	...	Y Y Y Y Y Y Y	Mem	Y	III	−2.76	Diskless	Ha− WHa(DM)=1.47 DM#25
LOri 022	...	Y Y Y Y Y Y Y	Mem	Y	III	−2.65	Diskless	Ha− WHa(DM)=4.39 DM#44
LOri 023	...	Y Y Y Y Y Y Y	Mem	Y	III	−2.65	Diskless	Ha− WHa(DM)=1.95 DM#50
LOri 024	...	Y Y Y Y Y Y Y	Mem	Y	III	−2.67	Diskless	
LOri 025	...	Y Y Y Y Y Y Y	Mem?	Y	III	−2.72	Diskless	Ha− WHa(DM)=3.95 DM#59
LOri 026	...	Y Y Y Y Y Y Y	Mem	Y	III	−2.69	Diskless	Ha− WHa(DM)=6.07 DM#12
LOri 027	...	Y Y Y Y Y Y Y	Mem	Y	III	−2.68	Diskless	
LOri 028	...	Y Y Y Y Y Y Y	Mem?	Y	III	−2.67	Diskless	
LOri 029	...	Y Y Y Y Y Y Y	NM−	Y	II	−0.72	Thick	Ha+ WHa(DM)=30.00 DM#36
LOri 030	...	Y Y Y Y Y Y Y	Mem	Y	III	−2.60	Diskless	
LOri 031	M4.0	Y Y Y Y Y Y Y	Mem	Y	III	−2.69	Diskless	Ha− WHa=3.8 DM#20 WHa(DM)= 3.45
LOri 032	...	Y Y Y Y Y Y Y	Mem	Y	III	−2.64	Diskless	Ha− WHa(DM)=6.83 DM#55
LOri 033	...	Y Y Y Y Y Y Y	Mem	Y	III	−2.68	Diskless	Ha− WHa(DM)=3.14 DM#39
LOri 034	...	Y Y Y Y Y Y Y	NM−	Y	II	−0.85	Thick	Ha+ WHa(DM)=10.92 DM#33
LOri 035	...	Y Y Y Y Y Y Y	Mem	Y	III	−2.70	Diskless	Ha− WHa(DM)=4.13 DM#29
LOri 036	...	Y Y Y Y Y Y Y	Mem	Y	III	−2.67	Diskless	
LOri 037	...	Y Y Y Y Y Y Y	Mem	Y	III	−2.67	Diskless	Ha− WHa(DM)=3.63 DM#11
LOri 038	...	Y . Y Y Y . .	Mem	Y	I/II	−1.00	Thick	Ha+ WHa(DM)=24.95 DM#02
LOri 039	...	Y Y Y Y Y Y Y	Mem	Y	III	−2.65	Diskless	Ha− WHa(DM)=3.59 DM#49
LOri 040	...	Y Y Y Y Y Y Y	Mem	Y	III	−2.66	Diskless	Ha− WHa(DM)=3.90 DM#41
LOri 041	...	Y Y Y Y Y Y Y	Mem	Y	III	−2.69	Diskless	Ha− WHa(DM)=8.20 DM#38
LOri 042	M4.0	Y Y Y Y Y Y Y	Mem	Y	III	−2.67	Diskless	Ha− WHa=4.3 DM#54 WHa(DM)= 4.22
LOri 043	...	Y Y Y Y Y Y Y	Mem	Y	III	−2.69	Transition	
LOri 044	...	Y Y Y Y Y Y Y	Mem	Y	III	−2.65	Diskless	
LOri 045	...	Y Y Y Y Y Y Y	Mem	Y	II[e]	−2.68	Diskless	
LOri 046	...	Y Y Y Y Y Y Y	Mem?	Y	III	−2.67	Diskless	
LOri 047	...	Y Y Y Y Y Y Y	Mem	Y	III	−2.68	Diskless	Ha− WHa(DM)=8.65 DM#47
LOri 048	...	Y Y Y Y Y Y Y	Mem	Y	II	−2.07	Thin	
LOri 049	...	Y Y Y Y Y Y Y	Mem	Y	III	−3.32	Diskless	
LOri 050	M4.5	Y Y Y Y Y Y Y	Mem	Y	II	−0.60	Thick	200km WHa=15.6
LOri 051	...	Y Y Y Y Y Y Y	Mem	Y	III	−2.73	Diskless	
LOri 052	...	Y Y Y Y Y Y Y	Mem	Y	III	−2.68	Diskless	
LOri 053	...	Y Y Y Y Y Y Y	Mem	Y	III	−2.68	Diskless	
LOri 054	...	Y Y Y Y Y Y Y	Mem	Y	III	−2.68	Diskless	
LOri 055	M4.5:	Y Y Y Y Y Y Y	Mem	Y	III	−2.68	Diskless	Ha− WHa=8.2
LOri 056	M4.5:	Y Y Y Y Y Y Y	Mem	Y	III	−2.68	Diskless	Ha− WHa=7.2
LOri 057	M5.5	Y Y Y Y Y Y Y	Mem	Y	III	−2.62	Diskless	Ha− WHa=8.4
LOri 058	M4.5:	Y Y Y Y Y Y Y	Mem	Y	III	−3.16	Diskless	Ha− WHa=7.3
LOri 059	M4.5	Y Y Y Y Y Y Y	Mem	Y	III	−3.23	Diskless	Ha− WHa=8.7
LOri 060	M4.5:	Y Y Y Y Y Y Y	Mem	Y	III	−2.79	Diskless	Ha− WHa=4.1
LOri 061	...	Y Y Y Y Y Y Y	Mem	Y	II	−1.32	Thick	
LOri 062	...	Y Y Y Y Y Y Y	Mem	Y	II	−1.66	Thick	
LOri 063	M4.5:	Y Y Y Y Y Y Y	Mem?	Y	I/II	−1.58	Thick	Ha+FL WHa=12.8
LOri 064	...	Y Y Y Y Y Y Y	Mem	Y	III	−2.54	Thin	

TABLE 4—*Continued*

Name	Spectral Type	Phot. Mem.[a]	Paper I Mem.	Final Mem.	IRAC Classification[b]	SED Slope[c]	Disk Type	Comment[d]
LOri 065	...	Y Y Y Y Y Y	Mem	Y	III	−2.97	Transition	
LOri 066	...	Y Y Y Y Y Y	Mem	Y	III	−3.25	Diskless	
LOri 067	...	Y Y Y Y Y Y	Mem	Y	III	−2.83	Diskless	
LOri 068	M5.0	Y Y Y Y Y Y	Mem?	Y	III	−2.57	Diskless	Ha+ WHa=16.6
LOri 069	...	Y Y Y Y Y Y	Mem?	Y	III	−2.65	Diskless	
LOri 070	...	Y Y Y Y Y Y	Mem	Y	III	−2.57	Diskless	
LOri 071	M5.0	Y Y Y Y Y Y	Mem	Y	III	−2.58	Diskless	Ha− WHa=8.0
LOri 072	...	Y Y Y Y Y Y	Mem?	Y	III	−2.55	Thin	
LOri 073	M5.0	Y Y Y Y Y Y	Mem?	Y	III	−2.59	Diskless	Ha+? WHa=12.0
LOri 074	...	Y Y Y Y Y Y	Mem?	Y	III	−2.78	Diskless	
LOri 075	M5.5	Y Y Y Y Y Y	Mem?	Y	III	−2.67	Diskless	Ha− WHa=9.4 WHa=9.4
LOri 076	...	Y Y Y Y Y Y	Mem	Y	III	−2.62	Diskless	
LOri 077	M5.0	Y Y Y Y Y Y	Mem	Y	III	−2.72	Diskless	Ha− WHa=8.8
LOri 078	...	Y Y Y Y Y Y	Mem	Y	III	−2.58	Diskless	
LOri 079	...	Y Y Y Y Y Y	Mem?	Y	III	−2.51	Thin	
LOri 080	M5.5	Y Y Y Y Y Y	Mem	Y	II	−2.55	Thin	Ha+? WHa=14.3
LOri 081	M5.5	N Y Y Y Y Y	Mem+	Y	II	−1.70	Thick	Ha− WHa=4.2
LOri 082	M4.5	Y Y Y Y Y Y	Mem+	Y	II[e]	−2.82	Diskless	Ha− WHa=8.6
LOri 083	...	Y Y Y Y Y Y	Mem	Y	III	−2.85	Diskless	
LOri 084	...	Y Y Y Y Y Y	Mem	Y	III	−2.71	Diskless	
LOri 085	...	Y Y Y Y Y Y	Mem	Y	II	−1.63	Thick	
LOri 086	...	Y Y Y Y Y Y	Mem	Y	III	−2.86	Diskless	
LOri 087	M4.5	Y Y Y Y Y Y	Mem+	Y	III	−2.54	Thin	Ha− WHa=6.7
LOri 088	...	Y Y Y Y Y Y	Mem	Y	III	−2.58	Diskless	
LOri 089	M5.0	Y Y Y Y Y Y	Mem	Y	II	−2.50	Thin	Ha− WHa=5.1
LOri 090	...	Y Y Y Y Y Y	Mem	Y	III	−2.69	Diskless	
LOri 091	M5.5	Y Y Y Y Y Y	Mem	Y	II	−2.48	Thin	Ha+? WHa=14.7
LOri 092	...	Y Y Y Y Y Y	Mem	Y	II	−2.79	Diskless	
LOri 093	...	Y Y Y Y Y Y	Mem	Y	III	−2.68	Diskless	
LOri 094	M5.5	Y Y Y Y Y Y	Mem	Y	III	−2.82	Diskless	Ha− WHa=10.4
LOri 095	M6.0	Y Y Y Y Y Y	Mem+	Y	III	−2.91	Diskless	Ha− WHa=7.3
LOri 096	...	Y Y Y Y Y Y	Mem	Y	II	−1.71	Thick	
LOri 098	M5.0	Y Y Y Y Y Y	Mem+	Y	III	−2.61	Diskless	Ha− WHa=12.9
LOri 099	M5.25	Y Y Y Y Y Y	Mem	Y	III	−2.74	Diskless	Ha− WHa=6.6
LOri 100	M5.5	Y Y Y Y Y Y	Mem	Y	III	−2.67	Diskless	Ha+? WHa=13.1
LOri 101	...	N N ? ? Y Y	Mem?	N	III	−2.6	Diskless	
LOri 102	...	Y Y Y Y Y Y	Mem?	Y	III	−2.65	Diskless	
LOri 103	...	Y Y Y Y Y Y	Mem?	Y	III[f]	−2.31	Thin	
LOri 104	...	Y Y Y Y Y Y	Mem	Y	II	−1.30	Thick	
LOri 105	...	Y Y Y Y Y Y	Mem	Y	III	−2.75	Diskless	
LOri 106	M5.5	Y Y Y Y Y Y	Mem	Y	II	−1.16	Thick	Ha+ WHa=54.0
LOri 107	M6.0	Y Y Y Y Y Y	Mem+	Y	III	−2.68	Diskless	Ha− WHa=11.7
LOri 108	...	Y Y Y Y Y Y	Mem	Y	III	−2.61	Diskless	
LOri 109	M5.5	Y Y Y Y Y Y	Mem	Y	III	−2.82	Diskless	Ha− WHa=10.1
LOri 110.....	M5.5	Y Y Y Y Y Y	Mem	Y	II	−2.52	Thin	Ha− WHa=9.1
LOri 111.....	...	Y Y Y Y Y Y	Mem	Y	III	−3.19	Diskless	
LOri 112.....	...	Y Y Y Y Y Y	NM−	Y	III	−2.72	Diskless	
LOri 113.....	M5.5	Y Y Y Y Y Y	Mem	Y	II	−1.37	Thick	Ha+ WHa=22.0
LOri 114.....	M6.5	Y Y Y Y Y Y	Mem+	Y	II	−2.38	Thin	Ha− WHa=10.9
LOri 115.....	M5.0	Y Y Y Y Y Y	NM+	Y	II	−2.02	Thin	Ha− WHa=8.5
LOri 116.....	M5.5	Y Y Y Y Y Y	Mem+	Y	II	−2.43	Thin	Ha− WHa=11.1
LOri 117.....	M6.0	Y Y Y Y Y Y	Mem	Y	...	−2.20	Thin	Ha+? WHa=22.9
LOri 118.....	M5.5	Y Y Y Y Y Y	Mem+	Y	II	−1.37	Thick	Ha− WHa=10.1
LOri 119.....	M5.5	Y Y Y Y Y Y	NM?	Y	III	−2.85	Diskless	Ha+? WHa=12.7
LOri 120	M5.5	Y Y Y Y Y Y	Mem+	Y	II	−1.59	Thick	Ha− WHa=7.4
LOri 121	...	Y Y Y ? Y Y	NM−	Y	...	−2.31	Thin	
LOri 122	...	Y Y Y Y Y Y	Mem	Y	II	−2.46	Thin	
LOri 124	M5.5	Y Y Y Y Y Y	Mem?	Y	III	−2.56	Diskless	Ha− WHa=8.4
LOri 125	...	Y Y Y Y Y Y	NM−	Y	III	−2.56	Diskless	
LOri 126	M6.5	Y Y Y Y Y Y	Mem+	Y	II	−1.24	Thick	Ha+? WHa=26.2
LOri 127	...	N N N N N N	NM−	N	III	−2.78	Diskless	
LOri 128	...	Y Y Y Y Y Y	Mem?	Y	III	−2.69	Diskless	
LOri 129	M6.0	Y Y Y Y Y Y	Mem?	Y	II	−1.71	Thick	Ha+? WHa=12.1
LOri 130	M5.5	Y Y Y Y ? Y	Mem+	Y	III	−2.69	Diskless	Ha− WHa=8.7
LOri 131	...	Y Y Y Y Y Y	Mem?	Y	II	−2.12	Thin	

TABLE 4—*Continued*

Name	Spectral Type	Phot. Mem.[a]	Paper I Mem.	Final Mem.	IRAC Classification[b]	SED Slope[c]	Disk Type	Comment[d]
LOri 132	...	Y Y Y Y Y Y N	NM−	Y	II	−2.25	Thin	
LOri 133	M4.5	N N N ? ? N Y	NM+	N	...	−2.91	Diskless	
LOri 134	M5.0	Y Y Y Y ? ? Y	NM+	Y	III	−2.34	Thin	
LOri 135	M7.0	Y Y Y Y Y Y ?	Mem?	Y	III	−2.56	Diskless	Ha− WHa=15.5
LOri 136	...	Y Y Y Y Y Y Y	Mem?	Y	III	−2.17	Thin	
LOri 137	...	. N N . . .	?	N	...	...	...	
LOri 138	...	Y Y Y Y Y Y Y	NM−	Y	...	−2.13	Thin	
LOri 139	M6.0	Y Y Y Y Y Y Y	Mem+	Y	II	−1.22	Thick	Ha+? WHa=19.7
LOri 140	M7.0	Y Y Y Y Y Y Y	Mem+	Y	II	−1.40	Thick	Ha+ WHa=72.8
LOri 141	M4.5	N N ? N Y Y Y	NM+	N	...	−5.35	Diskless	
LOri 142	...	Y Y Y Y Y Y Y	Mem?	Y	...	...	...	
LOri 143	M6.5	Y Y Y Y Y Y Y	Mem+	Y	III	−2.59	Diskless	Ha+ WHa=35.7
LOri 144	...	N N N N N N Y	?	N?	...	...	...	
LOri 146	...	Y Y Y Y Y Y Y	Mem	Y	III	−1.90	Thin	
LOri 147	M5.5	Y Y ? N ? N Y	NM+	Y?	...	−2.41	Thin	
LOri 148	...	Y N Y Y Y Y N	NM−	Y?	...	−2.19	Thin	
LOri 149	...	. N N N . N .	?	N	...	...	...	
LOri 150	M8.0	Y Y Y Y Y Y Y	Mem+	Y	...	−2.72	Diskless	Ha− WHa=15.6
LOri 151	M5.5	N N N ? Y Y Y	NM?	N	...	...	...	
LOri 152	...	Y Y N N N N Y	NM−	N?	...	...	...	
LOri 153	...	? Y Y Y Y Y Y	?	Y	...	...	...	
LOri 154	M8.0	Y Y Y ? Y Y Y	Mem+	Y	...	...	...	Ha− WHa=16.9
LOri 155	M8.0	Y Y Y Y Y Y Y	Mem+	Y	III	−2.03	Thin	Ha+? WHa=38.0
LOri 156	M8.0	Y Y Y Y Y Y Y	Mem+	Y	III	−1.54	Thick	Ha+ WHa=101.7
LOri 157	...	N N N N N N Y	?	N	...	...	...	
LOri 158	...	N N N N N N Y	?	N?	...	...	...	
LOri 159	...	N N N N Y Y N	?	N?	...	...	...	
LOri 160	...	N Y Y Y Y Y Y	?	Y	...	...	...	
LOri 161	M8.5	Y Y Y Y Y Y Y	Mem+	Y	...	...	...	Ha+ WHa=123
LOri 162	...	Y Y Y Y Y Y Y	?	Y	...	...	...	
LOri 163	...	Y Y Y Y Y Y Y	?	Y	...	...	...	
LOri 164	...	N N . . N	?	N	...	...	...	
LOri 165	M7.5	N N Y Y Y Y ?	NM?	N?	...	...	...	
LOri 166	...	? ? Y N Y Y ?	?	Y?	...	...	...	
LOri 167	...	Y Y Y Y Y Y Y	?	Y	...	...	...	
LOri 168	...	N N . . . . Y	?	N?	...	...	...	
LOri 169	...	N N	?	Y?	...	...	...	
LOri 170	...	N N	?	N?	...	...	...	

[a] Membership is I vs. $(I-J)$; I vs. $(I-K)$; I vs. $(I-3.6)$; I vs. $(I-4.5)$; J vs. $(J-3.6)$; K vs. $(K-3.6)$; J vs. $(J-K)$.

[b] Classification as measured in the IRAC CCD: $[3.6]-[4.5]$ vs. $[5.8]-[8.0]$. Class III stands for diskless members, and Class II are classical T Tauri stars or substellar analogs.

[c] IRAC slope. Lada et al. (2006) classified the objects according to their IRAC slope: $\alpha < -2.56$ for a diskless object, $-2.56 < \alpha < -1.80$ for a transition object, and $\alpha > -1.80$ for objects bearing optically thick disks.

[d] Ha+ = $W(\mathrm{H}\alpha)$ above the saturation criterion. Ha− = $W(\mathrm{H}\alpha)$ below the saturation criterion; 200km = width of Hα equal to or larger than this value. WHa(DM) = from Dolan & Mathieu (2001).

[e] Probably diskless objects. The different results on IRAC CCD and IRAC slope are probably due to an uncertain measure at 5.8 μm.

[f] Probably a Class II source with an uncertain measure at 8.0 μm.

association. Figure 1 (after Allen et al. 2004; Megeath et al. 2004) displays the colors derived from the measurements at $[3.6]-[4.5]$, versus those obtained at $[5.8]-[8.0]$. This diagram produces an excellent diagnostic, allowing an easy discrimination between objects with and without disks. Note that due to the limiting magnitudes of the IRAC bands (see the discussion in the previous section), objects fainter than about $I = 18.6$ mag cannot have a complete set of IRAC colors and therefore cannot be plotted in the diagram. This fact imposes a limit on our ability to discover mid-IR excesses at the faint end of the cluster sequence. For λ Orionis cluster members, assuming a distance of 400 pc and an age of 5 Myr (and according to the models by Baraffe et al. 1998), this limit is located at 0.040 $M_{\odot}$. Figure 1 contains a substantial number of objects in the region corresponding to the Class II sources. In total, there are 31 objects located within the solid rectangle out of 134 λ Orionis members with data in the four IRAC bands. Among them, three (LOri 045, LOri 082, and LOri 092) possibly have relatively large photometric errors in their 5.8 μm flux because inspection of their spectral energy distributions (SEDs) indicates that they are likely diskless. Two additional objects, LOri 038 and LOri 063, have IRAC colors indicating Class I/II (actually, LOri 038 is very close to the Class II region). The SED (see below) indicates that both are Class II stars. Therefore, the fraction of cluster members that are Class II pre–main-sequence stars based on their IR excesses is ~22%–25%, for the spectral range M0–M6.5. This is different from what was inferred by Dolan & Mathieu (1999, 2001) and by us (Paper I), based on the distribution of the Hα emission and NIR CCDs. The *Spitzer*

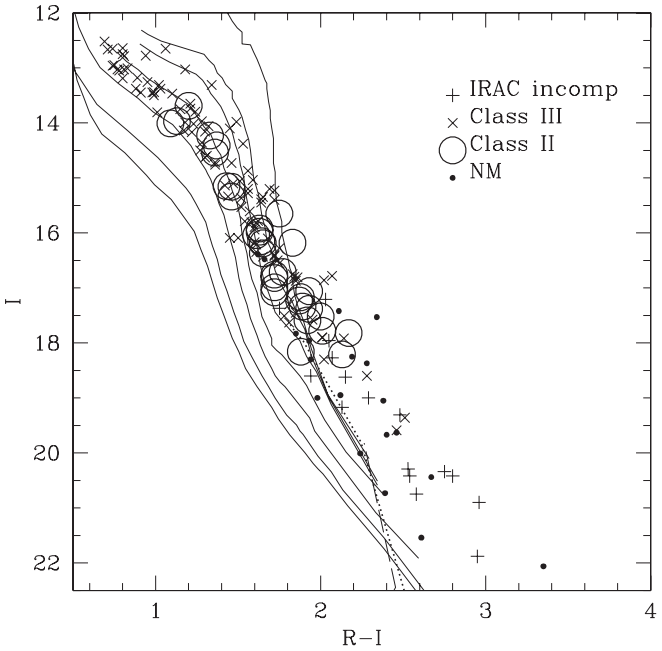

FIG. 4.—Optical CMD with the CFHT magnitudes and our new membership classification. Symbols as in previous figures. [*See the electronic edition of the Journal for a color version of this figure.*]

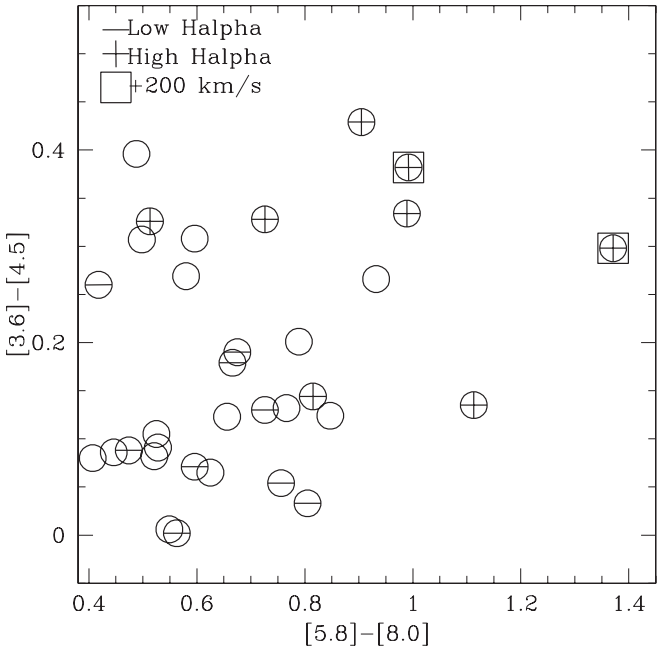

FIG. 5.—*Spitzer* IRAC CCD for Class II objects. We have included information regarding the Hα emission. [*See the electronic edition of the Journal for a color version of this figure.*]

IRAC data clearly demonstrate that the λ Orionis cluster does contain a significant number of stars with dusty circumstellar disks. No embedded objects (Class I) seem to be present, in agreement with the age range for the association (3–8 Myr or even slightly larger). Note that our different IR excess frequency compared to Dolan & Mathieu (1999, 2001) may result from their sample being primarily of higher mass stars than ours.

Figure 5 is a blowup of the region in Figure 1 corresponding to the Class II sources. We have also added big minus and plus signs, as well as large squares, to indicate those objects with measured Hα equivalent widths (in low- and medium-resolution spectrum). We have used the saturation criterion by Barrado y Navascués & Martín (2003) to distinguish between objects with high W(Hα) (*plus signs*) and normal W(Hα) (*minus signs*). In principal, an object with a W(Hα) value above the saturation criterion is either accreting or undergoing a flare episode. There are two-low mass stars (LOri 050 and LOri 063) with an Hα line broader than 200 km s^{-1} (Muzerolle et al. 2003), another independent indication of accretion (based on Natta et al. [2004], they should have very large accretion rates $\sim 10^{-9}\,M_{\odot}$ yr^{-1}). The theoretical disk models used to interpret the IRAC color-color diagram by Allen et al. (2004) suggest that the accretion rates increase from the bottom left to the top right of the figure. This is in agreement with our results, since most of the accreting objects (assuming that strong Hα is a good indicator of accretion) lie in the area of the figure with the larger excesses (*top right*). A couple of objects with very low Hα emission are located near the edge of the Class II area (*bottom left*), a fact that suggests that they may have a relatively thin disk, with small or negligible accretion. Actually these objects are surrounded by thin disks instead of thick primordial disks (see next section).

TABLE 5

LOCATION OF THE SUBSTELLAR FRONTIER, USING MODELS BY BARAFFE ET AL. (1998) AND A DISTANCE OF 400 pc

Age (Myr)	I_C	J	K_s	L'
1	16.72	14.35	13.32	12.88
3	17.18	14.87	13.84	13.40
5	17.55	15.36	14.35	13.92
8	17.92	15.80	14.80	14.36
10	18.13	16.01	15.01	14.57
16	18.52	16.40	15.40	14.96
20	18.71	16.59	15.60	15.15

NOTES.—Values such as 340 or 450 pc would modify the listed magnitudes by −0.35 and +0.26, respectively. We have included an interstellar reddening of $E(B-V) = 0.12$, equivalent to $A_I = 0.223$, $A_J = 0.106$, $A_K = 0.042$, and $A_L = 0.022$.

Regarding the brown dwarfs in the cluster, several probable members (LOri 126, LOri 129, LOri 131, LOri 132, LOri 139, and LOri 140) are located within the precinct of classical T Tauri stars. They are just at the border between stars and substellar objects, with magnitudes in the range $I = 17.52$–18.21 and $J = 15.38$–16.16 (the boundary is located at $I = 17.55$ and $J = 15.36$ for 5 Myr; see Table 5). In Paper I we presented low-resolution spectroscopy of LOri 126, LOri 139, and LOri 140, which suggests that they are cluster members (the spectral types are M6.5, M6.0, and M7.0 with an Hα equivalent width of 26.2, 19.7, and 72.8 Å, respectively). In addition, we have confirmed the membership of LOri 129 via medium-resolution spectroscopy (spectral type M6.0 with an Hα equivalent width of 12.1 Å).

In total, there are 15 brown dwarf candidates with a complete set of IRAC colors, 6 of which fall in the Class II region, thus making the fraction of brown dwarfs with IR colors indicative of circumstellar disks close to 40% (down to 0.04 $M_{\odot}$), similar to the 50% obtained by Bouy et al. (2007) in Upper Sco brown dwarfs using mid-IR photometry or the 50% derived by Guieu et al. (2006) in Taurus brown dwarfs with *Spitzer*.

4.2. *The Spectral Energy Distribution*

We have plotted the SEDs of our λ Orionis candidate members in Figures 6–8. There is clearly a range from approximately flat spectrum, to blackbody in the NIR but starting to show

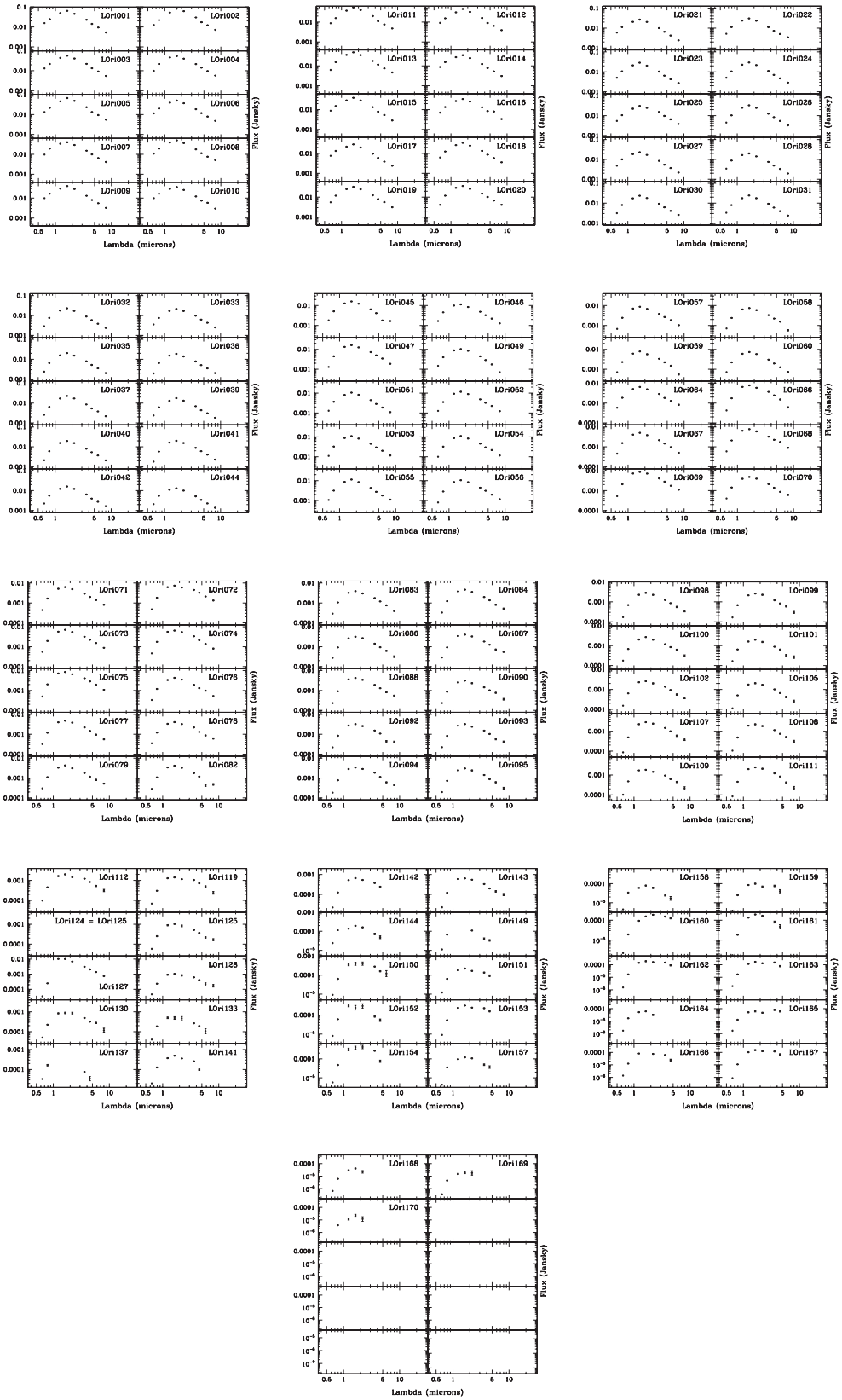

FIG. 6.— SEDs for some stellar members of the λ Orionis cluster sorted according to their IRAC slope: simple photosphere spectra. Objects lacking IRAC slope or being in the boundary between two types have been classified after visual inspection.

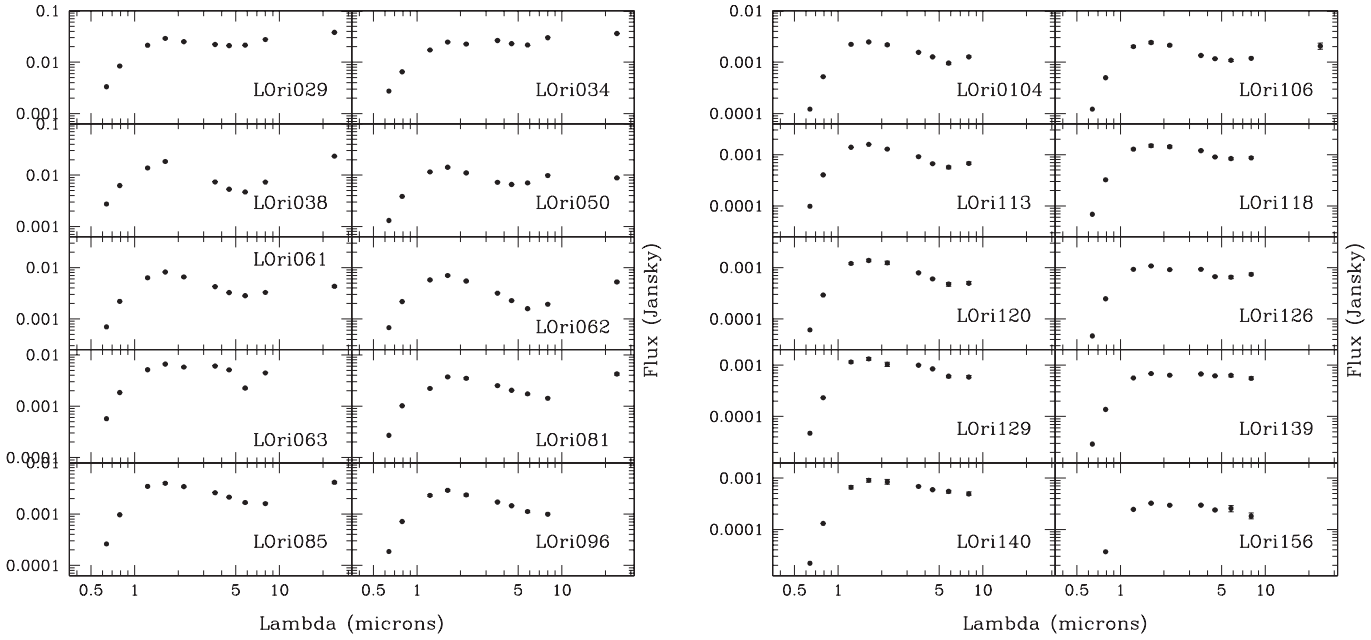

FIG. 7.—SED for some stellar members of the λ Orionis cluster sorted according to their IRAC slope: flat, or sloping IR spectra with the excess starting in the NIR (thick disks).

excesses at IRAC wavelengths, to only showing excess at 24 μm. A way to study the presence of a circumstellar disk around an object is to analyze the shape of the SED. After Lada et al. (2006), we have used the 3.6–8.0 μm slope for each source detected in at least three IRAC bands to distinguish between objects with optically thick, primordial disks, objects surrounded by optically thin or anemic disks, and objects without disks. The results of this test are presented in Table 4. In Figures 6–8 the SEDs are sorted in agreement with their IRAC slope classification: diskless objects (slope index or $\alpha < -2.56$) in Figure 6, thick disks ($\alpha > -1.8$) in Figure 7, and objects surrounded by thin disks ($-1.8 < \alpha < -2.56$) in Figure 8. In this last figure we also include two low-mass stars that present an excess only at 24 μm, due to a transition disk (see below). According to the IRAC slope, the fraction of cluster members detected in at least three of the IRAC bands with optically thick disks is 14%, while the total disk fraction is found to be 31% (similar to the 25% derived with the IRAC CCD). This fraction is lower than the 50% found by Lada et al. (2006) in IC 348 (1–3 Myr) as expected due to the different age of the clusters.

Figure 9 illustrates the evolution of the disk fraction with the age for several stellar associations (assuming that the infrared excess serves as a proxy of the presence of a circumstellar disk). The ratios for the different associations come from IRAC data (Hartmann et al. 2005; Lada et al. 2006; Sicilia-Aguilar et al. 2006) in order to avoid different results depending on the technique used (Bouy et al. 2007). The ratio for the λ Orionis cluster (Collinder 69) is about 30% and, as stated before, for the objects below the substellar borderline, the fraction of classical T Tauri objects seems to be larger. According to its older age, the thick-disk fraction in Collinder 69 is lower than that of IC 348 (this fraction is represented by open squares in Fig. 9).

Among the objects classified as Class III sources from Figure 1, only two (LOri 043 and LOri 065) have a measurement at [24] with an unambiguous detection. These two stars do not have excesses at 3.6 or 4.5 μm. Therefore, they can be classified as transition objects, the evolutionary link between the primordial disks and debris disks. A third of the Class II sources (11 out of 33) have measurements in the [24] band, all of them with clear excess, as

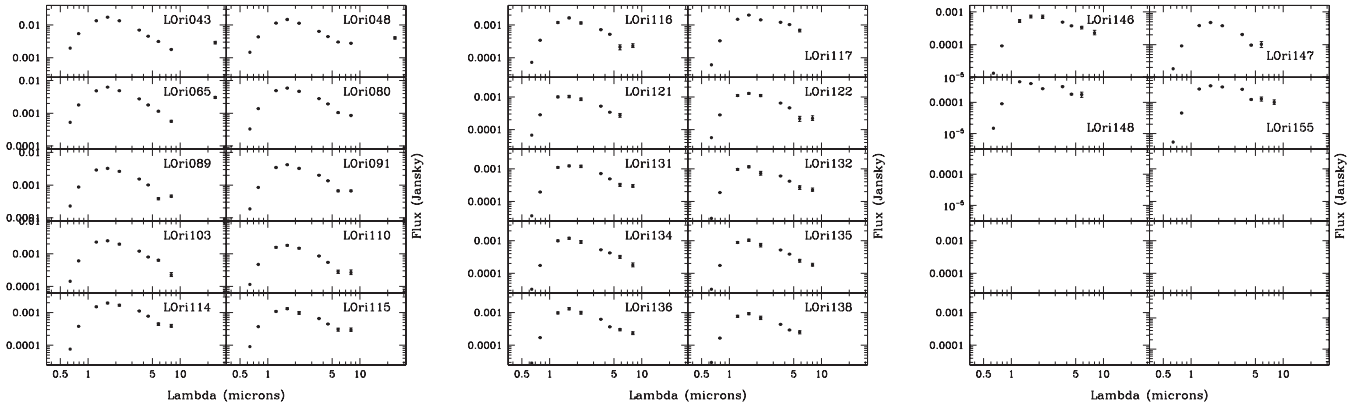

FIG. 8.—SED for some stellar members of the λ Orionis cluster sorted according to their IRAC slope: spectra with excesses beginning in the IRAC or MIPS range (thin disks and transition objects). LOri 043 and LOri 065 were classified as diskless objects but have been sorted as objects bearing thin disks due to their excess at MIPS [24].

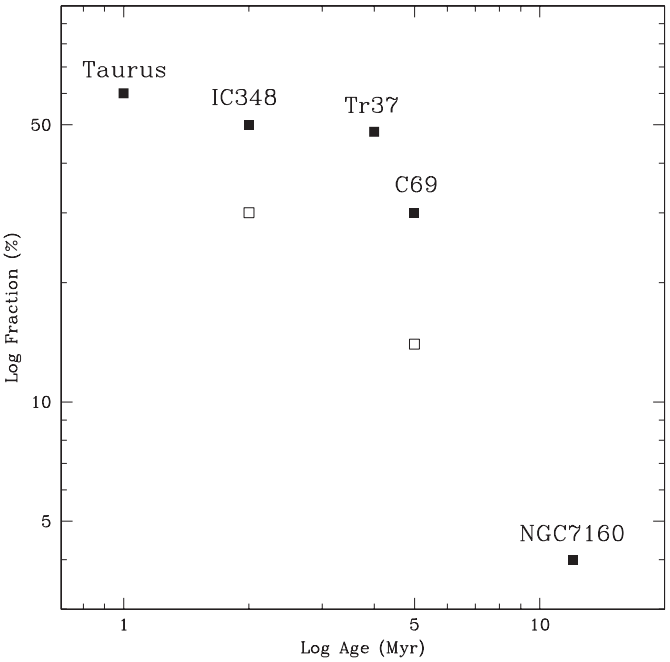

FIG. 9.—The fraction of Class II stars and massive brown dwarfs in several SFRs and young clusters (*filled squares*). Open squares stand for thick-disk fractions of IC 348 and Collinder 69.

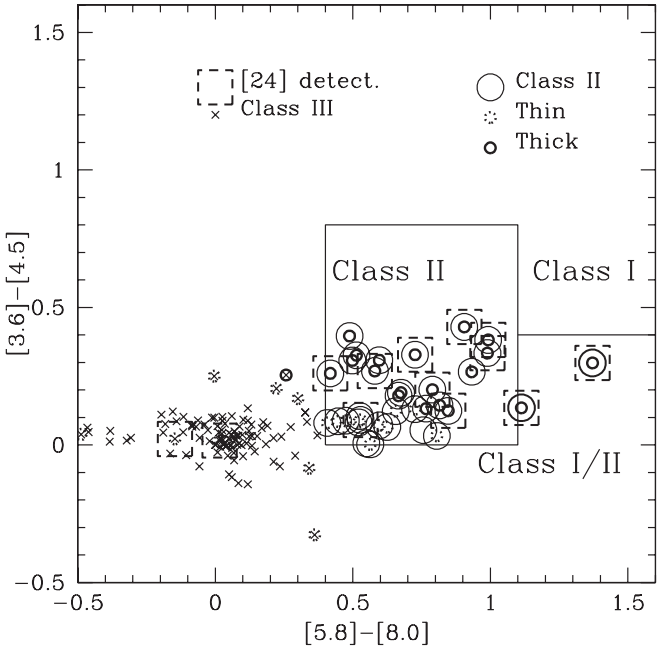

FIG. 10.—*Spitzer* IRAC CCD. We show with different symbols (see key) cluster members with different types of disks. [*See the electronic edition of the Journal for a color version of this figure.*]

expected from their Class II status. The lack of IR excesses at shorter wavelengths for LOri 043 and LOri 065 probably stems from an inner disk hole or at least less inner dust than for the Class II sources. Models of similar 24 μm–only excess sources and a discussion of their disk evolutionary significance can be found in Sicilia-Aguilar et al. (2006), Muzerolle et al. (2006), and D'Alessio et al. (2006). Figure 10 shows the same diagram as in Figure 1, but the MIPS 24 μm information is included as dashed squares. The small circles stand for objects having optically thin (*dashed circles*) or optically thick (*solid circles*) disks based on their IRAC slope. The diagram shows a smooth transition between the three types of objects: diskless, thin, and primordial disks. LOri 103 has a thin disk based on its 3.6–5.8 μm slope. It has been classified as Class III due to its magnitude at 8.0 μm, but we believe that it is actually a Class II source, and the faint magnitude at this bandpass is probably due to the presence of a nebulosity.

There are some objects classified as Class III sources by the IRAC CCD (they are outside, but close to, the Class II area in the diagram) but that have disks based on their IRAC slope. All these objects are brown dwarfs according to the models by Baraffe et al. (1998) (5 Myr) that pass all our membership criteria, and thus the ratio of substellar objects bearing disks increases to 50% (note that we need detections in at least three IRAC bands to calculate the IRAC slope).

None of our brown dwarf candidates have been detected at 24 μm. This is probably due to the detection limits for this band.

As a summary, of the 170 objects presented in Paper I, 167 are discussed here (the other three are spurious detections or the *Spitzer* photometry is not reliable). Excluding the sources classified as nonmembers, there are 22 that cannot be classified due to the incompleteness of the IRAC data, 95 have been classified as diskless, another two have transition disks, 25 thin disks, and 20 thick disks. All this information has been listed in Table 4. Note that there are nine objects classified as Class III from CCDs but that have thin disks according to the SED slopes, as well as another one (LOri 156, a very low mass brown dwarf candidate with a very intense Hα) that has a thick disk based on the slope of the IRAC data.

4.3. *The Spatial Distribution of the Members*

We have plotted the spatial distribution of our good candidate members in Figure 11. Four-point stars represent B stars and λ Orionis (O8 III). The Class III members (*crosses*) are approximately randomly distributed across the survey region. Both the Class II sources and the B stars give the impression of being concentrated into linear grouping, with most of the B stars being aligned vertically near R.A. = 83.8, and a large number of the Class II sources being aligned in the east-southeast direction (plus some less well-organized alignments running more or less north-south). It is possible that the spatial distributions are reflective of the birth processes in Collinder 69, with the youngest objects (the Class II sources and B stars) tracing the (former?) presence of dense molecular gas, whereas the Class III sources have had time to mix dynamically and they are no longer near the locations where they were born.

Figure 12 shows three different views of the central portion of the *Spitzer* mosaic at 3.6 μm for the Collinder 69 region. Figures 12*a* and 12*b* (with Fig. 12*b* being a blowup of the center of Fig. 12*a*) emphasize the distribution of Class II sources relative to the cluster center; Figure 12*c* shows the distribution of our brown dwarf candidates. The star λ Orionis is at the center of each of these figures. The object located south of the star λ Orionis is BD +09 879C (or HD 36861C, an F8 V star), with an angular distance of about 30″ from the close binary λ Orionis AB (the projected distance, if BD +09 879C is a cluster member, would be 12,000 AU from the AB pair). The apparent relative lack of cluster candidate members within about 75″ from the star λ Orionis may be illusory, as this region was "burned out" in the optical images of the CFHT 1999 survey and is also adversely affected in our IRAC images. There are a number of Class II sources at about 75″–90″ from λ Ori, corresponding to a projected separation of

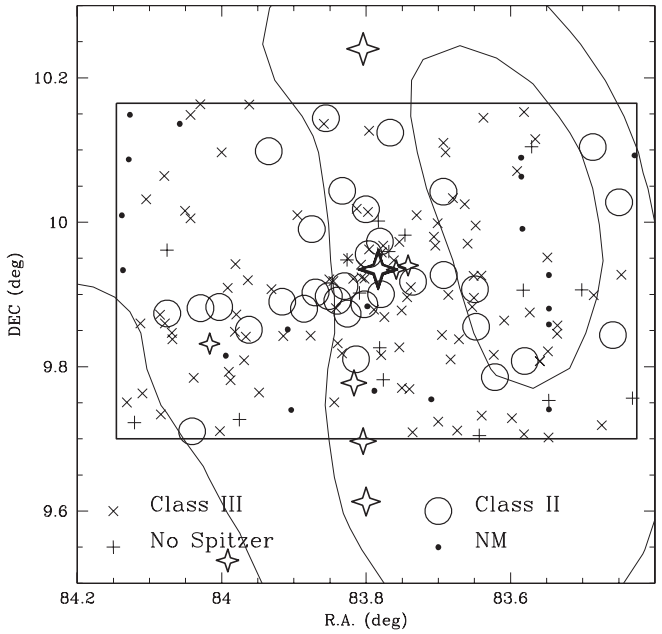

FIG. 11*a*

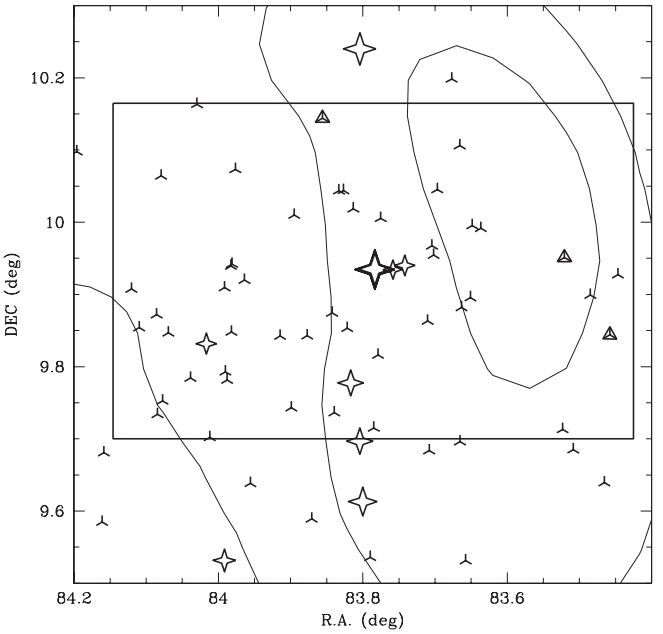

FIG. 11*b*

FIG. 11.—(*a*) Spatial distribution of our sample. *IRAS* contour levels at 100 μm also have been included as solid lines. The large rectangle corresponds to the CFHT survey (Paper I). Class II sources (classical T Tauri stars and substellar analogs) have been included as large open circles, whereas Class III (weak-line T Tauri) objects appear as crosses, and other λ Orionis members lacking the complete set of IRAC photometry are displayed with plus signs. (*b*) Spatial distribution of the low-mass stars from Dolan & Mathieu (1999, 2001). OB stars appear as four-point stars, with size related to magnitude (the bigger, the brighter). The overplotted thick triangles indicate those stars whose Hα equivalent width is larger than the saturation criterion defined by Barrado y Navascués & Martín (2003), thus suggesting the presence of active accretion. Based on Hα alone, the fraction of accreting stars would be 11%. [*See the electronic edition of the Journal for a color version of this figure*.]

order 30,000 AU, so at least at that distance circumstellar disks can survive despite the presence of a nearby O star.

Regarding the distribution of brown dwarfs, a significant number of them (30%) are within the inner circle with a diameter of 9′ (our original optical survey covered an area of $42' \times 28'$). However, there are substellar members at any distance from the star λ Ori (Fig. 12*c*), and there is no substantial evidence that the cluster brown dwarfs tend to be close to the massive central star.

We have estimated the correlation in spatial distribution of different sets of data: Class II versus Class III candidates, objects with any kind of disk (thin, thick, and transition) versus diskless objects, and stellar versus substellar objects (following the substellar frontier given in Table 5 for different ages and bands). We have computed the two-sided Kuiper statistic (invariant Kolmogorov-Smirnov test) and its associated probability that any of the previously mentioned pairs of stellar groups were drawn from the same distribution. We have calculated the two-dimensional density function of each sample considering a $4.5' \times 3'$ grid binning in a $45' \times 30'$ region centered at $05^{h}35^{m}08.31^{s}$, $+09^{\circ}56'03.6''$ (the star λ Orionis). The test reveals that in the first case, the cumulative distribution function of Class II candidates is significantly different from that of Class III candidates, with a probability for these data sets being drawn from the same distribution of ~1%. This situation changes when comparing the set of objects harboring any kind of disk with that of diskless objects, finding a probability of ~50% in this case (and hence no conclusion can be drawn, other than that there is no strong correlation). On the other hand, regarding a correlation with age, the test points out a trend in the relationship between the spatial distribution of stellar and substellar objects depending on the assumed age. The value of the probability of these two populations sharing a common spatial distribution decreases from ~30% when assuming an age of 3 Myr to ~0.001% for an age of 8 Myr. The value assuming an age of 5 Myr is ~1%.

The spatial distribution of objects detected at 24 μm can be seen in Figure 13. The nebulosity immediately south of the star λ Orionis (close to BD +09 879C) corresponds to the H II region LBN 194.69−12.42 (see the detail in Fig. 12*b* in the band [3.6]). Most of the detected members are located within the inner 9′ circle, with an apparent concentration in a "filament" running approximately north-south (i.e., aligned with the B stars as illustrated in Fig. 11*b*). Out of the cluster members discovered by Dolan & Mathieu (1999, 2001), 11 are within the MIPS [24] image (see Fig. 13) and have fluxes above the detection level. The closest member to λ Orionis is DM 33 (LOri 034), about 2′ east from the central star.

The MIPS image at 24 μm suggests that there are two bubbles centered around the λ Orionis multiple star (actually, the center might be the C component or the H II region LBN 194.69−12.42). The first one is about 25′ away, and it is located along the northeast/southwest axis. More conspicuous is the smaller front located at a distance of 10.75′, again centered on the H II region and not in λ Orionis AB. In this case, it is most visible located in the direction west/northwest, opposite to the alignment of Class II objects and low-mass members with excess at 24 μm. Similar structures can be found at larger scales in the *IRAS* images of this region, at 110′ and 190′.

The star 37 Ori, a B0 III, is located at the center of the cocoon at the bottom of the image. The source IRAS 05320+0927 is very close and it is probably the same.

Note that while BD +09 879C would appear to be the source of a strong stellar wind and/or large UV photon flux, it is not obvious that the visible star is the UV emitter because the spectral type for BD +09 879C is given as F8 V (Lindroos 1985). It would

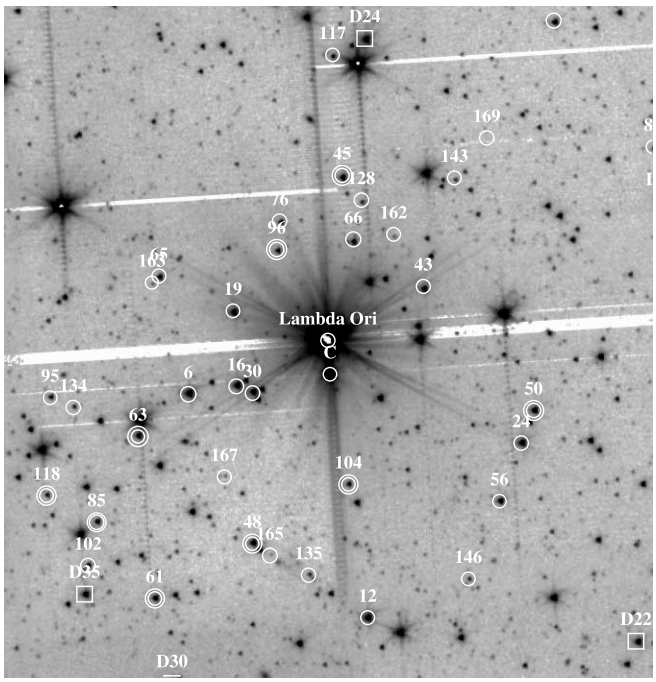

FIG. 12*a*

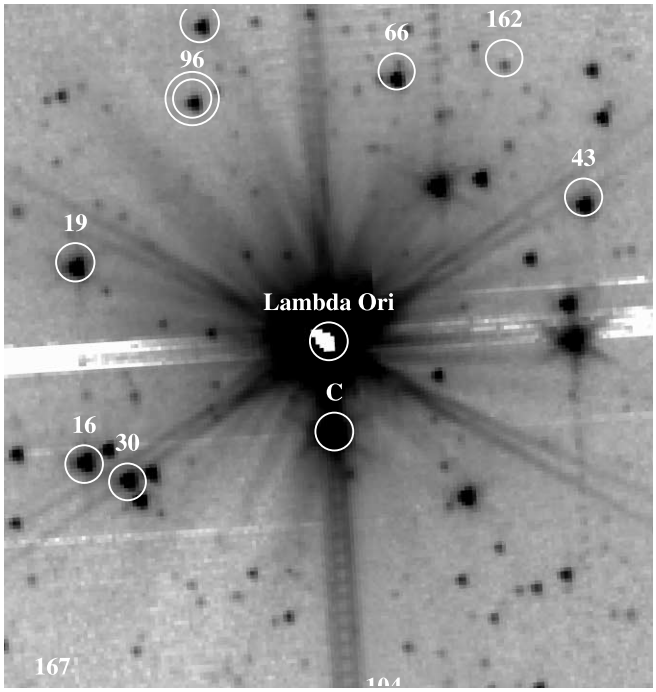

FIG. 12*b*

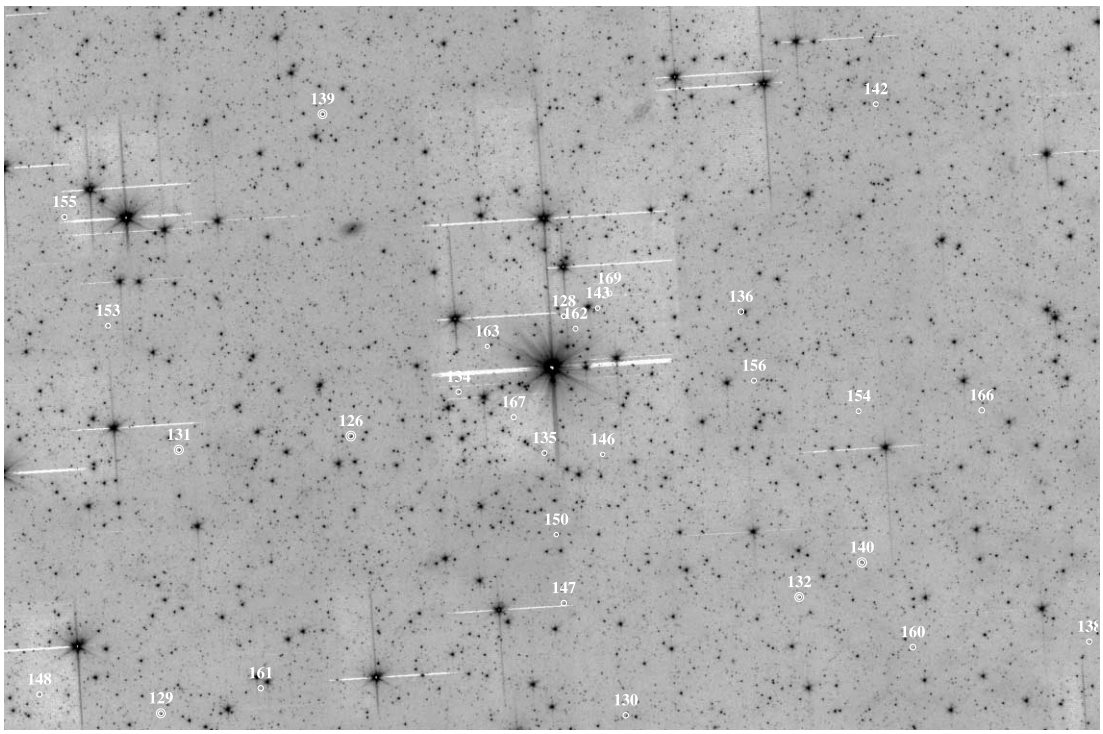

FIG. 12*c*

FIG. 12.—*Spitzer* IRAC image at 3.6 μm centered around the star λ Orionis. (*a*) The size is about $9' \times 9'$, equivalent to 192,000 AU. The double circle indicates the presence of a Class II object, whereas squares indicate the location of cluster members from Dolan & Mathieu (1999, 2001). The intensity of the image is in logarithmic scale. (*b*) Detail around the star λ Orionis. The size is about $3.3' \times 3.3'$, equivalent to 80,000 AU. (*c*) Distribution of bona fide brown dwarfs. The size of the image is $45' \times 30'$. North is up, east is left.

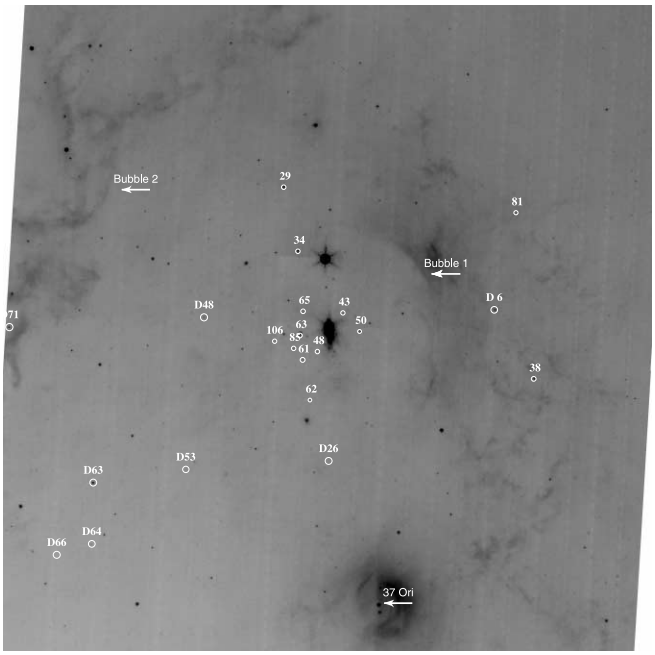

FIG. 13.—*Spitzer* MIPS image at 24 μm, which includes the members of the λ Orionis cluster visible at this wavelength, including those cluster members by Dolan & Mathieu (1999, 2001) as large circles and CFHT members as small circles detected at this wavelength. The size is about $60.5' \times 60.5'$. North is up, east is left. The figure is centered on the star λ Ori AB.

be useful to examine this star more closely in order to try to resolve this mystery.

5. CONCLUSIONS

We have obtained *Spitzer* IRAC and MIPS data of an area about 1 deg^2 around the star λ Orionis, the central star of the 5 Myr λ Orionis open cluster (Collinder 69). These data were combined with our previous optical and NIR photometry (from 2MASS). In addition, we have obtained deep NIR imaging. The samples have been used to assess the membership of the 170 candidate members, selected from Barrado y Navascués et al. (2004).

By using the *Spitzer* IRAC data and the criteria developed by Allen et al. (2004) and Hartmann et al. (2005), we have found 33 objects that can be classified as classical T Tauri stars and substellar analogs (Class II objects). This means that the fraction of members with disks is 25% and 40%, respectively, for the stellar (in the spectral range M0–M6.5) and substellar population (down to 0.04 $M_\odot$). However, by combining this information with Hα emission (only a fraction of them have spectroscopy), we find that some do not seem to be accreting.

Moreover, as expected from models, we see a correlation in the $[3.6] - [4.5]$ versus $[5.8] - [8.0]$ diagram for objects with redder colors (more IR excess) to have stronger Hα emission. In addition, following Lada et al. (2006) and the classification based on the slope of the IRAC data, we found that the ratio of substellar members bearing disks (optically thin or thick) is $\sim$50%, whereas it is about 31% for the complete sample (14% with thick disks). This result suggests that the timescale for primordial disks to dissipate is longer for lower mass stars, as suggested in Barrado y Navascués & Martín (2003).

We have also found that the distribution of Collinder members is very inhomogeneous, specifically for the Class II objects. Most of them are located in a filament that goes from the central star λ Orionis to the southeast, more or less toward the dark cloud Barnard 35. In addition, there are several Class II stars close to the central stars. If the (previously) highest mass member of Collinder 69 has already evolved off the main sequence and become a supernova, either the disks of these Class II stars survived that episode or they formed subsequent to the supernova.

We have also derived the fluxes at 24 μm from *Spitzer* MIPS imaging. Only a handful (13) of the low-mass stars were detected (no brown dwarfs). Most of them are Class II objects. In the case of the two Class III members with 24 μm excess, it seems that they correspond to transition disks, already evolving toward the protoplanetary phase.

We thank Calar Alto Observatory for allocation of director's discretionary time to this programme. This research has been funded by Spanish grants MEC/ESP2004-01049, MEC/Consolider-CSD2006-0070, and CAM/PRICIT-S-0505/ESP/0361.

REFERENCES

Allen, L. E., et al. 2004, ApJS, 154, 363
Baraffe, I., Chabrier, G., Allard, F., & Hauschildt, P. H. 1998, A&A, 337, 403
———. 2002, A&A, 382, 563
Barrado y Navascués, D., Bayo, A., Morales Calderón, M., Huélamo, N., Stauffer, J. R., & Bouy, H. 2007, A&A, in press
Barrado y Navascués, D., Huélamo, N., & Morales Calderón, M. 2005a, Astron. Nachr., 326, 981
Barrado y Navascués, D., & Martín, E. L. 2003, AJ, 126, 2997
Barrado y Navascués, D., Stauffer, J. R., & Bouvier, J. 2005b, in The Initial Mass Function 50 Years Later, ed. E. Corbelli & F. Palle (Dordrecht: Springer), 133
Barrado y Navascués, D., Stauffer, J. R., Bouvier, J., Jayawardhana, R., & Cuillandre, J.-C. 2004, ApJ, 610, 1064 (Paper I)
Bouy, H., Huélamo, N., Martín, E. L., Barrado y Navascués, D., Sterzik, M., & Pantin, E. 2007, A&A, 463, 641
Briceño, C., Luhman, K. L., Hartmann, L., Stauffer, J. R., & Kirkpatrick, J. D. 2003, in IAU Symp. 211, Brown Dwarfs, ed. E. Martín (San Francisco: ASP), 81
Chabrier, G., Baraffe, I., Allard, F., & Hauschildt, P. 2000, ApJ, 542, 464
Cutri, R. M., et al. 2003, 2MASS All Sky Catalog of Point Sources (NASA/IPAC Infrared Science Archive)
D'Alessio, P., Calvet, N., Hartmann, L., Franco-Hernández, R., & Servín, H. 2006, ApJ, 638, 314
Dolan, C. J., & Mathieu, R. D. 1999, AJ, 118, 2409
———. 2001, AJ, 121, 2124
Engelbracht, C. W., et al. 2007, PASP, in press
Fazio, G. G., et al. 2004, ApJS, 154, 10
Guieu, S., Dougados, C., Monin, J.-L., Magnier, E., & Martín, E. L. 2006, A&A, 446, 485
Hartmann, L. 2004, in IAU Symp. 221, Star Formation at High Angular Resolution, ed. M. Burton, R. Jayawardhana, & T. Bourke (San Francisco: ASP), 201
Hartmann, L., et al. 2005, ApJ, 629, 881
Harvey, P. M., et al. 2006, ApJ, 644, 307
Hunt, L. K., et al. 1998, AJ, 115, 2594
Lada, C. J., et al. 2006, AJ, 131, 1574
Lindroos, K. P. 1985, A&AS, 60, 183
Luhman, K. L. 2004, ApJ, 617, 1216
Makovoz, D., & Khan, I. 2005, in ASP Conf. Ser. 347, Astronomical Data Analysis Software and Systems XIV, ed. P. Shopbell, M. Britton, & R. Ebert (San Francisco: ASP), 81
McCaughrean, M. J., & Stauffer, J. R. 1994, AJ, 108, 1382
Megeath, S. T., et al. 2004, ApJS, 154, 367
Muzerolle, J., Hillenbrand, L., Calvet, N., Briceño, C., & Hartmann, L. 2003, ApJ, 592, 266
Muzerolle, J., et al. 2006, ApJ, 643, 1003
Natta, A., et al. 2004, A&A, 424, 603
Reach, W. T., et al. 2005, PASP, 117, 978
Rieke, G. H., et al. 2004, ApJS, 154, 25
Sicilia-Aguilar, A., Hartmann, L. W., Hernández, J., Briceño, C., & Calvet, N. 2005, AJ, 130, 188
Sicilia-Aguilar, A., et al. 2006, ApJ, 638, 897